

Effect of Extended Benzannelation Orientation on Bergman and Related Cyclizations of Isomeric Quinoxalenediynes

Stephanie A. Valenzuela, Alondra J. Cortes, Zakery J. E. Tippins, Morgan H. Daly, Terrell E. Keel, Benjamin F Gherman, and John D. Spence

J. Org. Chem., **Just Accepted Manuscript** • DOI: 10.1021/acs.joc.7b02420 • Publication Date (Web): 09 Nov 2017

Downloaded from <http://pubs.acs.org> on November 10, 2017

Just Accepted

“Just Accepted” manuscripts have been peer-reviewed and accepted for publication. They are posted online prior to technical editing, formatting for publication and author proofing. The American Chemical Society provides “Just Accepted” as a free service to the research community to expedite the dissemination of scientific material as soon as possible after acceptance. “Just Accepted” manuscripts appear in full in PDF format accompanied by an HTML abstract. “Just Accepted” manuscripts have been fully peer reviewed, but should not be considered the official version of record. They are accessible to all readers and citable by the Digital Object Identifier (DOI®). “Just Accepted” is an optional service offered to authors. Therefore, the “Just Accepted” Web site may not include all articles that will be published in the journal. After a manuscript is technically edited and formatted, it will be removed from the “Just Accepted” Web site and published as an ASAP article. Note that technical editing may introduce minor changes to the manuscript text and/or graphics which could affect content, and all legal disclaimers and ethical guidelines that apply to the journal pertain. ACS cannot be held responsible for errors or consequences arising from the use of information contained in these “Just Accepted” manuscripts.



Effect of Extended Benzannelation Orientation on Bergman and Related Cyclizations of Isomeric Quinoxalenediynes

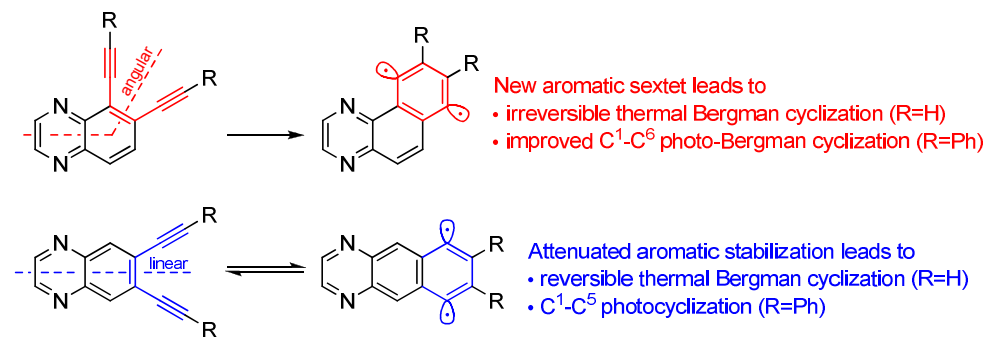
Stephanie A. Valenzuela, Alondra J. Cortés, Zakery J. E. Tippins, Morgan H. Daly, Terell E.

Keel, Benjamin F. Gherman* and John D. Spence*

Department of Chemistry, California State University, Sacramento, 6000 J Street, Sacramento, California, 95819, United States

*Corresponding authors gbermanb@csus.edu; jspence@csus.edu

Table of Contents/Abstract Graphic



Abstract

A combined computational and experimental study was conducted to examine the effect of extended benzannelation orientation on C¹-C⁵ and C¹-C⁶ cyclization of acyclic quinoxalenediynes. Calculations (mPW1PW91/cc-pVTZ // mPW1PW91/6-31G(d,p)) on terminal and phenylethynyl-substituted 5,6-diethynylquinoxaline and 6,7-diethynylquinoxaline showed C¹-C⁶ Bergman cyclization as the favored thermodynamic reaction pathway, with larger C¹-C⁶ preference for the angular quinoxalenediynes due to gain of a new aromatic sextet.

1
2
3 Kinetic studies, as a function of 1,4-cyclohexadiene concentration, revealed retro-Bergman ring
4 opening predominates over hydrogen atom abstraction ($k_{-1} > k_2$) for 6,7-diethynylquinoxaline
5 while 5,6-diethynylquinoxaline undergoes irreversible Bergman cyclization indicative of a large
6 retro-Bergman ring opening barrier ($k_2 > k_{-1}$). The effect of extended linear versus angular
7 benzannelation on reaction pathway shows in the contrasting photocyclizations of phenylethynyl
8 derivatives. While angular 5,6-diethynylquinoxalines gave exclusive C¹-C⁶ photocyclization,
9 linear 6,7-diethynylquinoxaline afforded C¹-C⁵ fulvene products. Computed singlet-triplet gaps
10 and biradical stabilization energies indicated weak interaction between the nitrogen lone pair and
11 proximal radical center in angular 5,6-diethynylquinoxalines. The overall data indicates
12 extended angular benzannelation effectively renders Bergman cyclization irreversible due to
13 favorable aromatic stabilization energy, while extended linear benzannelation results in increased
14 retro-Bergman ring opening, allowing C¹-C⁵ cyclization to become a competitive reaction
15 channel.
16
17
18
19
20
21
22
23
24
25
26
27
28
29
30
31
32
33
34
35
36
37
38
39
40
41
42
43
44
45
46
47
48
49
50
51
52
53
54
55
56
57
58
59
60

Introduction

Intramolecular diradical cyclizations of conjugated polyunsaturated systems have become powerful additions to the arsenal of ring-forming processes.¹ The prototypical examples include C¹-C⁶ Bergman² and C¹-C⁵ Schreiner-Pascal³ cyclizations of enediynes along with C²-C⁷ Myers-Saito⁴ and C²-C⁶ Schmittel⁵ cyclizations of enyne-allenes (Figure 1). In particular, Bergman cyclization has been extensively studied due to the ability of natural products such as calicheamicin and dynemicin to cleave DNA upon cyclization of an enediyne unit.⁶ In addition to the development of synthetic antitumor agents,⁷ diradical cyclizations have found applications as a synthetic tool in the preparation of novel polycyclic aromatic systems,⁸ in the preparation of polymeric materials,⁹ in the construction of molecular electronic nanodevices on surfaces,¹⁰ and may serve as precursors to the formation of aromatic species in interstellar medium.¹¹ Furthermore, diradical cyclizations have provided a challenging platform towards the development of computational models due to the multiconfigurational nature of diradical species.¹²

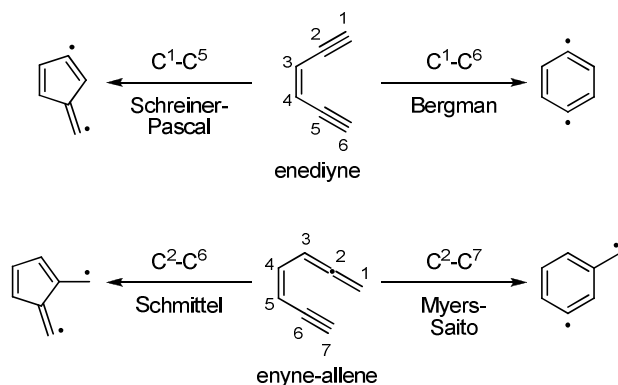


Figure 1. Diradical cyclization pathways of enediynes and enyne-allenes.

1
2
3 For the parent enediyne, (*Z*)-hex-3-ene-1,5-diyne, C¹-C⁶ Bergman cyclization is the
4 preferred thermal reaction pathway, where gain of an aromatic sextet places the *p*-benzyne
5 diradical intermediate in a deep energy well.¹³ Incorporating the enediyne alkene within a
6 benzene ring, however, increases endothermicity of C¹-C⁶ cyclization as the aromaticity gain
7 upon converting 1,2-diethynylbenzene to naphthalene is attenuated.¹⁴ As a result, 1,2-
8 diethynylbenzene has a lower barrier towards retro-Bergman ring opening, making cyclization to
9 the diradical reversible.¹⁵

10
11
12 Experimentally, these energetic changes are manifested in a measured rate of
13 disappearance for 1,2-diethynylbenzene that becomes dependent upon hydrogen atom donor
14 concentration and provides the overall rate constant, k_{obs} , under pseudo-first order conditions.¹⁶
15 In comparison, the rate of disappearance of simple non-benzannelated acyclic enediynes are
16 independent of hydrogen atom donor concentration and directly provide the rate of Bergman
17 cyclization, k_1 .¹⁷ This critical difference for benzannelated enediynes makes comparison of
18 literature data on Bergman cyclization kinetics complicated as the concentration of hydrogen
19 atom donor is highly variable across the available experimental data. This trend continues upon
20 extended benzannelation as Bergman cyclization of 2,3-diethynylnaphthalene also exhibits a rate
21 dependence on hydrogen atom donor concentration.¹⁶ In this case, however, the measured
22 disappearance rate is two-fold slower compared to 1,2-diethynylbenzene with higher
23 concentrations of hydrogen atom donor required to detect formation of cyclized product.

24
25
26 Unfortunately, the increased endothermic cost upon benzannelation of an enediyne
27 cannot readily be offset through traditional substituent effects in the annealed ring. Upon C¹-C⁶
28 cyclization, the developing diradicals are orthogonal to the π -system of the benzene ring
29 preventing direct conjugation between radical centers and substituents. This is evident by the
30
31
32
33
34
35
36
37
38
39
40
41
42
43
44
45
46
47
48
49
50
51
52
53
54
55
56
57
58
59
60

1
2
3 fact that *para*-substituents on 1,2-diethynylbenzene have minor effects on Bergman cyclization
4 rates operating through relatively weak field effects.¹⁸ The challenge of tuning enediyne
5 cyclization is further complicated by the presence of two orthogonal π -systems wherein changes
6 to the in-plane π -system (conversion to σ -bond and two radical centers) control the reaction
7 barrier while changes to the out-of-plane π -system (gain of aromaticity) can influence overall
8 reaction energy.¹⁹ One approach to control the rate of Bergman cyclization of benzannelated
9 enediynes is through reactant destabilization imparted by *ortho*-substituents.²⁰ Here, steric
10 compression of the alkynes increases electron repulsion of the in-plane π -system in the reactant
11 that is alleviated in the transition state. A more extreme route to tune enediyne reactivity through
12 benzannelated substituents employs cyclization of enediyne radical anions.²¹ Under such
13 conditions, radical anionic cyclization of enediynes is accelerated upon benzannelation with
14 increased sensitivity to remote substituents due to crossing of out-of-plane and in-plane
15 molecular orbitals near the transition state. In comparison, phenyl groups located on the alkyne
16 termini are more sensitive to substituent effects as direct conjugation to the in-plane π -system is
17 available. For example, electron withdrawing groups present in 1,2-bis(4-
18 nitrophenylethynyl)benzene were found to lower the C¹-C⁶ activation barrier compared to
19 electron rich *para*-methoxyphenyl substituents.²² Overall, however, substituent effects on
20 phenylethynyl groups have been much less studied as placement of phenyl groups on the alkyne
21 termini significantly raises the barrier towards C¹-C⁶ Bergman cyclization.²³ Furthermore, bulky
22 phenylethynyl substituents can lead to phenyl-shifted products²⁴ and competing C¹-C⁵
23 cyclization facilitated by gain of resonance stabilization to one of the radical centers from the
24 external phenyl group.²⁵

1
2
3
4
5
6
7
8
9
10
11
12
13
14
15
16
17
18
19
20
21
22
23
24
25
26
27
28
29
30
31
32
33
34
35
36
37
38
39
40
41
42
43
44
45
46
47
48
49
50
51
52
53
54
55
56
57
58
59
60

In a previous study we reported computational data on diethynylquinoxaline isomers to further probe the influence of extended benzannelation orientation on Bergman cyclization energetics.²⁵ Calculations revealed that endothermicity of Bergman cyclization to the corresponding diradical intermediate can increase or decrease relative to 1,2-diethynylbenzene ($\Delta H_{\text{rxn}} = 9.2$ kcal/mol) based on the nature of the extended aromatic core. With extended linear benzannelation, as in 6,7-diethynylquinoxaline **1** (Figure 2), Bergman cyclization becomes less thermodynamically favorable ($\Delta H_{\text{rxn}} = 12.3$ kcal/mol) as the aromatic stabilization gained upon cyclization is further attenuated. In comparison, Bergman cyclization of 5,6-diethynylquinoxaline **2** is less endothermic ($\Delta H_{\text{rxn}} = 5.4$ kcal/mol) and approaches the calculated value for (*Z*)-hex-3-ene-1,5-diyne ($\Delta H_{\text{rxn}} = 0.88$ kcal/mol) as a new aromatic sextet is produced, restoring aromatic stabilization to the angularly fused diyl product. These results are consistent with the earlier experimental observation that 2,3-diethynyl-naphthalene undergoes a more sluggish Bergman cyclization compared to 1,2-diethynylbenzene, likely due to rapid retro-Bergman cyclization.¹⁶ Unfortunately, no experimental data is available on 1,2-diethynyl-naphthalene to directly compare this effect.

Despite these changes to the reaction energy profile, aromatic or heteroaromatic cores are commonly utilized when conducting photo-Bergman cyclization²⁶ to prevent *cis-trans* isomerization of the enediyne alkene. For example, the seminal work of Turro *et al.*²⁷ and Funk *et al.*²⁸ employed benzannelated enediynes in the photocyclization of acyclic and cyclic enediynes, respectively. Subsequently, Jones *et al.*²⁹ and Hiramama *et al.*³⁰ locked the central double bond within an alicyclic ring to demonstrate that aromatic cores are not strictly required for successful photo-Bergman cyclization of acyclic enediynes. Interestingly, although direct comparisons were not made, the isolated yield of photoadduct derived from 1,2-

1
2
3 bis(phenylethynyl)cyclohexene (22%) reported by Jones is higher than values typically reported
4
5 for 1,2-bis(phenylethynyl)benzene (1-10%).^{24,31} Funk also noted increased conversion of an
6
7 angular naphthalene-fused enediyne over the corresponding linear isomer, again suggesting
8
9 aromatic stabilization can influence photo-Bergman cyclization yields. Based on our previous
10
11 calculations, along with available literature data, the nature of extended benzannelation can
12
13 provide unique opportunities to tune enediyne cyclization energetics.
14
15

16
17 In the present paper we report the syntheses, computational studies, kinetic studies, and
18
19 photochemical reactivity of a series of diethynylquinoxalines to directly compare the effect of
20
21 linear versus angular extended benzannelation on enediyne reactivity (Figure 2). Calculations
22
23 were conducted on unsubstituted 6,7- and 5,6-diethynylquinoxalines **1** and **2** along with bis-
24
25 phenylethynylquinoxaline isomers **3** and **4** to examine changes in reaction energetics along the
26
27 C¹-C⁶ and C¹-C⁵ reaction channels. Kinetic studies, as a function of 1,4-cyclohexadiene
28
29 concentration, were then conducted on terminal quinoxalenediynes **1** and **2** to gain experimental
30
31 data to support our calculations. Finally, photochemical reactivity was examined on
32
33 phenylethynyl quinoxalenediynes **3-6** to determine if a change in extended benzannelation
34
35 orientation manifests in improved photo-Bergman cyclization yields for quinoxalenediynes.
36
37
38
39
40
41
42
43
44
45
46
47
48
49
50
51
52
53
54
55
56
57
58
59
60

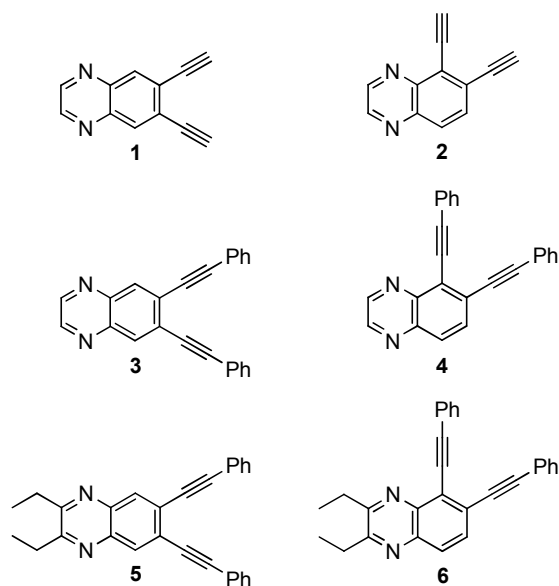


Figure 2. Quinoxalenediynes **1–6**.

Results and Discussion

Computational Analysis. A. C¹–C⁵ Cyclization Products. Prior to examining reaction energetics, relative enthalpies (Table 1) and relative free energies (Table S3) were calculated for the isomeric diyls derived from C¹–C⁵ cyclization of quinoxalenediynes **1–4** (Figure 3). For linear derivatives **1** and **3**, symmetry in the starting enediyne leads to one possible C¹–C⁵ cyclization pathway, providing a mixture of *E/Z* diradical intermediates. However, angular derivatives **2** and **4** lack symmetry and have two possible C¹–C⁵ cyclization pathways leading to a total of four possible isomeric diradical intermediates. For terminal quinoxalenediynes **1** and **2**, the lowest energy isomers calculated for C¹–C⁵ cyclization were the corresponding *Z*-diradical isomers **1-Z** and **2-Z**, respectively.^{3a} For phenyl-substituted quinoxalenediynes **3** and **4**, however, optimization of the *E/Z* C¹–C⁵ diradical isomers yielded the same structure in which the exocyclic fulvene radical adopts a virtually 180° bond angle (177.4° in **3-Lin**, 176.3° in **4-Lin**, and 174.3° in **4'-Lin**) leading to essentially linear intermediates which lean 3–6° towards

the *Z*-isomer. As a result, optimization of isomers **1-Z** and **1-E** derived from **3** both lead to **3-Lin**. Similarly, optimization of **2-Z/E** and **2'-Z/E** derived from **4** provided **4-Lin** and **4'-Lin**, respectively. A similar geometrical outcome was noted by Alabugin *et al.* in geometry optimizations of the C¹-C⁵ cyclization products derived from diaryl-substituted 1,2-diethynylbenzene derivatives.³² The linearization of the radical center is attributed to conjugation with the terminal aryl group and consequent rehybridization of the radical center. The lowest energy isomers derived from C¹-C⁵ cyclization of **1-4** (**1-Z** for **1**, **3-Lin** for **3**, **2-Z** for **2**, and **4-Lin** for **4**) were then used in the computation of the cyclization reaction energetics.

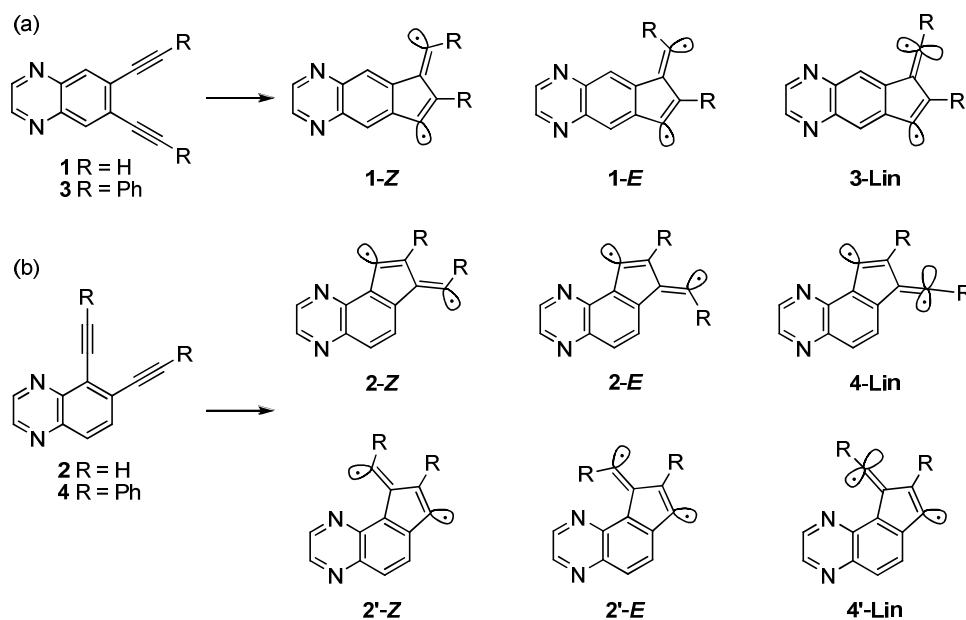


Figure 3. Isomers derived from C¹-C⁵ cyclization of (a) linear quinoxalenediynes **1** and **3** and (b) angular quinoxalenediynes **2** and **4**.

Table 1. Relative Enthalpies (25 °C, gas phase, kcal/mol) for C¹-C⁵ Cyclization of **1-4** and Corresponding Boltzmann Percentages (Cf. structures in Figure 3)

Substrate	Products
-----------	----------

linear	1-Z	1-E	3-Lin			
1 (R=H)	0 (96.11%)	1.90 (3.89%)	n/a			
3 (R=Ph)	n/a	n/a	0 (100%)			
angular	2-Z	2-E	4-Lin	2'-Z	2'-E	4'-Lin
2 (R=H)	-0.27 (53.31%)	1.93 (1.30%)	n/a	0 (33.90%)	0.64 (11.49%)	n/a
4 (R=Ph)	n/a	n/a	-0.23 (59.51%)	n/a	n/a	0 (40.49%)

B. Cyclization Reaction Energetics. To gain insight into the effect of extended benzannelation orientation and alkyne substitution pattern on C¹-C⁶ and C¹-C⁵ cyclization energetics, we examined activation enthalpy barriers and reaction enthalpies for quinoxalenediynes **1-4** computationally, with the results summarized in Table 2 (free energy barriers and reaction free energies provided in Table S1). From the data, several interesting trends emerge.

Table 2. Computed Cyclization Thermodynamic Parameters (25 °C, gas phase, kcal/mol)

Substrate	C ¹ -C ⁵		C ¹ -C ⁶		(C ¹ -C ⁵)-(C ¹ -C ⁶)	
	ΔH^\ddagger	ΔH_{rxn}	ΔH^\ddagger	ΔH_{rxn}	$\Delta\Delta H^\ddagger$	$\Delta\Delta H_{\text{rxn}}$
linear						
1 (R = H)	39.07	31.46	31.16	12.27	7.91	19.19
3 (R = Ph)	38.21	30.92	43.07	27.42	-4.86	3.50

angular						
2 (R = H)	40.26	32.61	30.32	5.50	9.94	27.11
4 (R = Ph)	40.16	32.68	42.36	21.11	-2.20	11.57
linear-angular						
1 - 2	-1.19	-1.15	0.84	6.77		
3 - 4	-1.95	-1.76	0.71	6.31		

First, substitution of the terminal alkynes in **1** and **2** with phenyl groups has little effect on reaction barrier or reaction energies along the C¹–C⁵ cyclization channel. Apparently, any increased steric hindrance from phenyl substitution is compensated by the gain of resonance stabilization to the developing exocyclic vinyl radical center.^{3b} Upon C¹–C⁶ cyclization, however, increased steric interactions from the addition of phenyl substituents cannot be offset by resonance stabilization of the developing diradical. As a result, introduction of phenyl substituents increases the C¹–C⁶ activation barrier by approximately 12 kcal/mol and reaction energy by 15–16 kcal/mol for **3** and **4** compared to **1** and **2**, respectively.

Second, when comparing C¹–C⁵ versus C¹–C⁶ reaction pathways for unsubstituted derivatives **1** and **2**, C¹–C⁶ Bergman cyclization is favored kinetically and thermodynamically. However, upon phenyl substitution in **3** and **4**, increased sterics leads to C¹–C⁵ becoming the preferred reaction channel kinetically while aromatic stabilization in the C¹–C⁶ product results in Bergman cyclization remaining the preferred thermodynamic reaction pathway. Overall, the thermodynamic preference for C¹–C⁶ cyclization is more pronounced with the angular derivatives **2** and **4** primarily due to formation of a new aromatic sextet in these cases.²⁵

Nucleus-independent chemical shift calculations (NICS (Table S4) and NICS-1 (Table 3)) confirm increased aromaticity in the newly formed 6-membered ring produced upon C¹–C⁶ cyclization of the angular quinoxalenediynes compared to their linear counterparts. The NICS-1 data reveal that the new aromatic sextet generated in **2** and **4** has aromaticity 7.9% greater and

11.1% greater than the 6-membered ring formed upon C¹-C⁶ cyclization of **1** and **3**, respectively. In addition, similar NICS-1 values at the transition states upon C¹-C⁶ cyclization for the linear and angular analogs provide support for the small $\Delta\Delta H^\ddagger$ values calculated between **1** and **2** and between **3** and **4** (cf. Table 2). Furthermore, larger NICS-1 values for the C¹-C⁶ cyclization products derived from **2** and **4** support larger $\Delta\Delta H_{\text{rxn}}$ values calculated between the linear and angular quinoxalenediyne derivatives. In comparison, NICS-1 calculations on the newly formed 5-membered rings produced upon C¹-C⁵ cyclization of **1-4** confirm the negligible aromaticity gain along the C¹-C⁵ reaction channel. Similar NICS and NICS-1 calculations from Schreiner *et al.* on (*Z*)-hex-3-ene-1,5-diyne and 1,2-diethynylbenzene likewise showed appreciable aromaticity in the Bergman cyclization transition states.^{13a} Further, the decrease in the NICS-1 value from the formation of the new aromatic sextet in *p*-benzyne compared to the Bergman product formed from the benzannelated reactant 1,2-diethynylbenzene is comparable to, though somewhat smaller than, that calculated here between the Bergman cyclization of angular quinoxalenediynes **2** and **4** and linear counterparts **1** and **3**.

Table 3. Calculated NICS-1 Values^a for the 5- and 6-Membered Rings Formed in the Cyclization Reactions of 1-4

Substrate	C ¹ -C ⁵		C ¹ -C ⁶	
	transition state	product	transition state	product
1 (R = H)	-1.5	-2.2	-9.6	-11.9
2 (R = H)	-1.3	-1.9	-9.9	-12.9
3 (R = Ph)	-1.2	-1.7	-7.6	-10.2
4 (R = Ph)	-0.8	-1.3	-8.2	-11.4

^aThe NICS-1 value for the *p*-benzyne diradical singlet at the same level of theory is -12.6.

Finally, when examining the effect of linear versus angular extended benzannelation, the data indicates steric hindrance combined with aromatic stabilization energy can influence

1
2
3 cyclization energetics and reaction pathway. For terminal quinoxalenediynes, derivatives **1** and
4
5 **2** both favor C^1-C^6 over C^1-C^5 cyclization as the lower barrier pathway (by 7.9–9.9 kcal/mol) as
6
7 well as the more energetically favorable reaction channel (by 19.2–27.1 kcal/mol). For each
8
9 parameter, angular quinoxalenediyne **2** has a stronger preference for C^1-C^6 cyclization which
10
11 produces a new aromatic sextet. Furthermore, for **1** and **2** the retro C^1-C^5 barrier (~7.6 kcal/mol)
12
13 is significantly lower than the corresponding retro C^1-C^6 barrier (18.9–24.8 kcal/mol), with the
14
15 C^1-C^6 retro-Bergman barrier of angular derivative **2** the highest retro-barrier calculated in this
16
17 study, again highlighting the importance of the new aromatic sextet in the angularly fused
18
19 product. Supporting this data, terminal quinoxalenediynes **1** and **2** exclusively undergo C^1-C^6
20
21 Bergman cyclization under thermal conditions (*vide infra*). When examining the effect of
22
23 extended linear versus angular benzannelation on phenylethynyl derivatives **3** and **4**, however,
24
25 the situation is not as clear. For the linear derivative **3**, addition of phenyl substituents leads to
26
27 C^1-C^5 becoming the preferred kinetic pathway (favored by 4.9 kcal/mol) and, while C^1-C^6
28
29 remains the preferred thermodynamic channel (favored by 3.5 kcal/mol), attenuated aromatic
30
31 stabilization gain and increased steric hindrance leads to this isomer having the smallest reaction
32
33 enthalpy favoring C^1-C^6 . In comparison, angular phenyl-substituted **4** has a small C^1-C^5 kinetic
34
35 preference (favored by 2.2 kcal/mol), while the gain of a new aromatic sextet leads to C^1-C^6
36
37 Bergman cyclization being the preferred thermodynamic reaction channel (favored by 11.6
38
39 kcal/mol). Overall, from this data one may anticipate aromatic stabilization along the C^1-C^6
40
41 channel for angular quinoxalenediyne **4** to be the dominant energetic factor leading to a
42
43 successful photo-Bergman cyclization. However, photolysis of linear quinoxalenediyne **3**, with
44
45 the smallest retro-Bergman ring opening barrier, is less predictable and may lead to a mixture of
46
47 cyclization products.
48
49
50
51
52
53
54
55
56
57
58
59
60

C. Cyclization Reaction Electronics. In addition to aromatic stabilization energy, electronic interactions between the proximal nitrogen atom and the enediyne π -orbitals or developing diyl intermediate can also influence reaction energetics for angular quinoxalenediynes.

Upon examining the reactant angular quinoxalenediynes, Mulliken charge populations reveal a small repulsion between the nitrogen atom (-0.493) and the proximal alkyne π -bond (-0.181) in angular derivative **2**. In comparison, for **4**, the charge on the nitrogen atom is nearly equal (-0.499) to that in **2**, while the charge on the proximal alkyne π -bond in **4** is significantly smaller (-0.039), leading to minimal repulsion. For both **2** and **4**, however, this electronic repulsion has little impact on the geometry of the enediyne functional group (Table 4). For example, the C¹-C⁶ distances and enediyne bond angles (as measured from the mid-point of alkyne to mid-point of alkene to mid-point of alkyne) are nearly equal for quinoxalenediynes **1**-**4**. In addition, the alkyne bond lengths and bond orders are equal between **1** and **2** and between **3** and **4**.

Table 4. Geometric Parameters for Quinoxalenediynes 1–4

Substrate	C ¹ -C ⁶ distances (Å)	alkyne bond length ^a (Å)	enediyne bond angle ^b	Wiberg bond order ^a
1 (R = H)	4.126	1.208	89.90°	2.822
2 (R = H)	4.136	1.208, 1.208	89.31°	2.810, 2.817
3 (R = Ph)	4.086	1.214	90.50°	2.654
4 (R = Ph)	4.145	1.214, 1.215	89.11°	2.638, 2.646

^aAlkyne bond lengths and bond orders are identical due to symmetry in **1** and **3**. For **2** and **4**, the alkyne proximal to the N atom is listed first.

^bMeasured in the enediyne functional unit from mid-point of alkyne to mid-point of alkene to mid-point of alkyne.

To probe the effect of the nitrogen atoms on the diyl intermediates, we examined biradical stabilization energies (BSE) and singlet–triplet (S–T) splittings for quinoxalenediynes **1–4** along the C¹–C⁵ and C¹–C⁶ reaction channels (Figure 4). Close spatial proximity between the nitrogen atom and one of the radical centers in the angular diyl intermediates can affect the BSE and S–T gap,³³ each of which provide estimates of through bond coupling in the diyl.³⁴ As a result, any electronic effect from the proximal nitrogen atom in the angular quinoxalenediynes may be indirectly monitored by relative changes in the BSE and S–T gap compared to the linear derivative. First, the C¹–C⁶ cyclization product derived from **1** has a S–T gap and BSE comparable to *p*-benzyne,^{35,36} 1,4-naphthalene,^{35,36} and 5,8-quinolyne,³³ with BSE values underestimating the S–T gap as previously observed.³⁶ However, for the C¹–C⁶ cyclization product derived from angular quinoxalenediynes **2**, both the S–T gap and BSE are lower, which suggests through space interaction between the nitrogen lone pair and the proximal radical that weakens the through bond orbital interaction between the two radical centers. The phenyl-substituted derivatives **3** and **4** similarly show a decrease in the S–T gap and BSE in going from the linear to the angular C¹–C⁶ product, although the values for the S–T gap and BSE are overall smaller compared to **1** and **2**. Second, the C¹–C⁵ product **1-Z** has a larger S–T gap and BSE compared to the C¹–C⁶ product from **1** as expected due to the anti-periplanar geometry of the radical centers in **1-Z**.³⁶ In addition, the C¹–C⁵ cyclization product **2-Z** also has a larger S–T gap and BSE versus the C¹–C⁶ cyclization product from **2**. However, there is not as significant of a difference for the S–T gap and BSE between **1** and **2** along the C¹–C⁵ channel compared to the C¹–C⁶ channel as the distance from the proximal radical carbon to the nitrogen atom in the diradical products from **2** is 0.21 Å greater in the C¹–C⁵ than in the C¹–C⁶ pathway (Table 5) which minimizes any interactions. As with the C¹–C⁶ reaction channel, the C¹–C⁵ products **3-**

1
2
3 **Lin** and **4-Lin** from the phenyl-substituted derivatives also show smaller S–T gaps and BSEs
4
5 than **1-Z** and **2-Z**. However, the decrease in the S–T gap is greater than that seen along the C¹–
6
7 C⁶ channel upon phenyl substitution, as along the C¹–C⁵ channel the exocyclic radical centers in
8
9 **3-Lin** and **4-Lin** rehybridize and gain resonance stabilization with the phenyl group, thereby
10
11 reducing the through bond coupling.
12
13
14
15
16
17
18
19
20
21
22
23
24
25
26
27
28
29
30
31
32
33
34
35
36
37
38
39
40
41
42
43
44
45
46
47
48
49
50
51
52
53
54
55
56
57
58
59
60

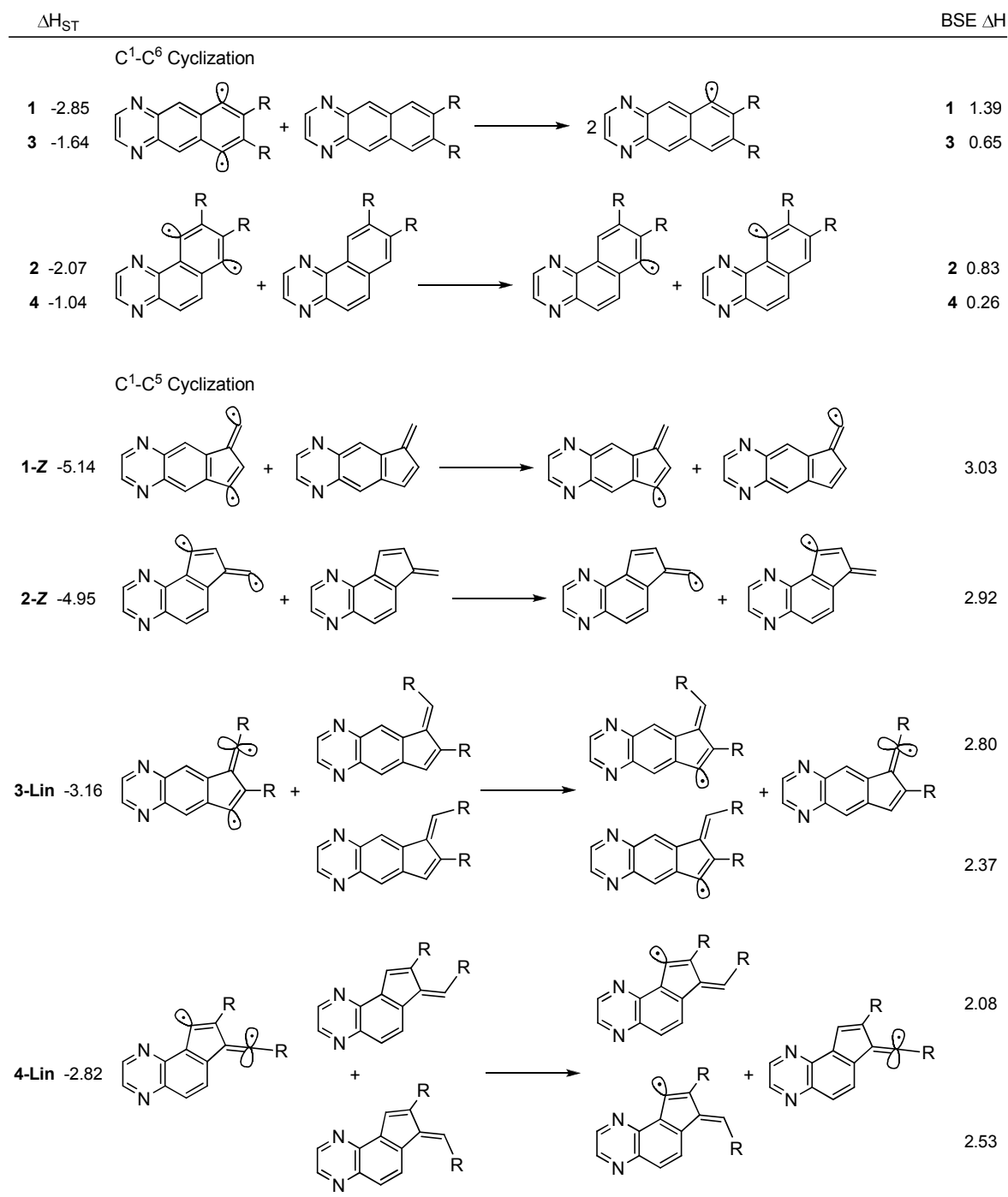


Figure 4. Singlet–triplet splitting (kcal/mol) and biradical stabilization energies (kcal/mol) of cyclization products from quinoxalenediynes 1–4.

Table 5. Distance Between Proximal Nitrogen Atom of the Quinoxaline Group and Carbon Radical (Å) During Cyclization Reactions of **2 and **4****

	2 (R = H)	4 (R = Ph)
C ¹ -C ⁵ TS	3.028	3.019
C ¹ -C ⁵ PRD	3.086	3.080
C ¹ -C ⁶ TS	2.856	2.860
C ¹ -C ⁶ PRD	2.878	2.888

The interaction between the radical sites in the diyl intermediates and the proximal nitrogen atom influences, to a small yet discernable degree, the reactivity of the angular quinoxalenediynes. For the C¹-C⁶ pathway transition states and products, the Mulliken charge populations (Table 6) show that the carbon radical proximal to the nitrogen atom bears a more positive charge (difference ranging from +0.037 to +0.064) in the angularly fused cases compared to the linear analogs, while the carbon radical distal to the nitrogen atom bears a more negative charge (difference ranging from -0.015 to -0.025). This represents a small step towards zwitterionic character for the C¹-C⁶ diradical³⁷ in the angularly fused cases, and stabilization for the slightly greater development of the cationic center is provided by the spatially aligned lone pair of the proximal nitrogen atom in the Bergman cyclization product of **2** and **4**. For **4**, this effect leads to a lower activation enthalpy ($\Delta\Delta H^\ddagger = -0.71$ kcal/mol vs. linear) and contributes to the lower reaction enthalpy ($\Delta\Delta H_{\text{rxn}} = -6.31$ vs linear). In **2** though, this effect combines with the destabilization of reactant **2** to give larger differences versus the linear analog ($\Delta\Delta H^\ddagger = -0.84$ kcal/mol and $\Delta\Delta H_{\text{rxn}} = -6.77$ vs. linear). The dominant energetic contribution to the $\Delta\Delta H_{\text{rxn}}$ values, though, remains aromaticity gain upon C¹-C⁶ cyclization of **2** and **4**. For the C¹-C⁵ pathway transition states and products, the Mulliken charge populations (Table 6) show that the carbon radical proximal to the nitrogen atom bears only a slightly more positive charge (difference ranging from +0.029 to +0.038) in the angularly fused cases compared to the linear

analogs. Again, this can be explained by the greater separation between the nitrogen atom and the proximal radical center in the C¹-C⁵ cyclization pathway, minimizing any stabilization of zwitterionic resonance structures by the nitrogen lone pair.

Table 6. Mulliken Charge Populations for Carbon Radicals During Cyclization Reactions for 1-4^a

	R=H (2)		R=H (1)		R=Ph (4)		R=Ph (3)	
	C Radical Proximal to N	C Radical Distal to N	C Radical Proximal to N	C Radical Distal to N	C Radical Proximal to N	C Radical Distal to N	C Radical Proximal to N	C Radical Distal to N
C ¹ -C ⁵ TS	0.006	-0.309	-0.032	-0.302	-0.091	0.000	-0.126	0.015
C ¹ -C ⁵ PRD	0.016	-0.221	-0.013	-0.225	-0.059	0.028	-0.088	0.033
C ¹ -C ⁶ TS	0.077	-0.012	0.013	0.013	0.001	-0.081	-0.063	-0.063
C ¹ -C ⁶ PRD	0.025	-0.036	-0.012	-0.012	-0.007	-0.066	-0.052	-0.052

^aData for the nitrogen proximal to the carbon radical are provided in Table S5.

Finally, the Mulliken spin populations at the transition states (Table 7) for the radical carbons in the angularly-fused C¹-C⁵ reaction are larger (more so for **4** vs. **3** compared to **2** vs. **1**) than for the linear analogs, indicating more radical delocalization in the linear cases. The essentially identical C¹-C⁵ distances in the transition states between **1** and **2** ($\Delta C^1-C^5 = 0.004 \text{ \AA}$) and between **3** and **4** ($\Delta C^1-C^5 = 0.001 \text{ \AA}$) suggests the spin population differences are not due to differences in timing of the transition states along the reaction coordinate. The greater spin delocalization for the linear derivatives contributes to the C¹-C⁵ cyclization becoming less kinetically favorable for **2** vs. **1** ($\Delta\Delta H^\ddagger = +1.19 \text{ kcal/mol}$) and **4** vs. **3** ($\Delta\Delta H^\ddagger = +1.95 \text{ kcal/mol}$), where the latter value is larger due to the greater difference in radical delocalization in **3** vs. **4** compared to **1** vs. **2**.

Table 7. Mulliken Spin Populations for the Carbon Radicals During the Cyclization Reactions for 1–4^a

	R=H (2)		R=H (1)		R=Ph (4)		R=Ph (3)	
	C Radical Proximal to N	C Radical Distal to N	C Radical Proximal to N	C Radical Distal to N	C Radical Proximal to N	C Radical Distal to N	C Radical Proximal to N	C Radical Distal to N
C ¹ –C ⁵ TS	-0.620	0.629	0.598	-0.620	-0.617	0.476	0.572	-0.455
C ¹ –C ⁶ TS	0.289	-0.286	0.319	-0.319	-0.589	0.583	-0.600	0.600

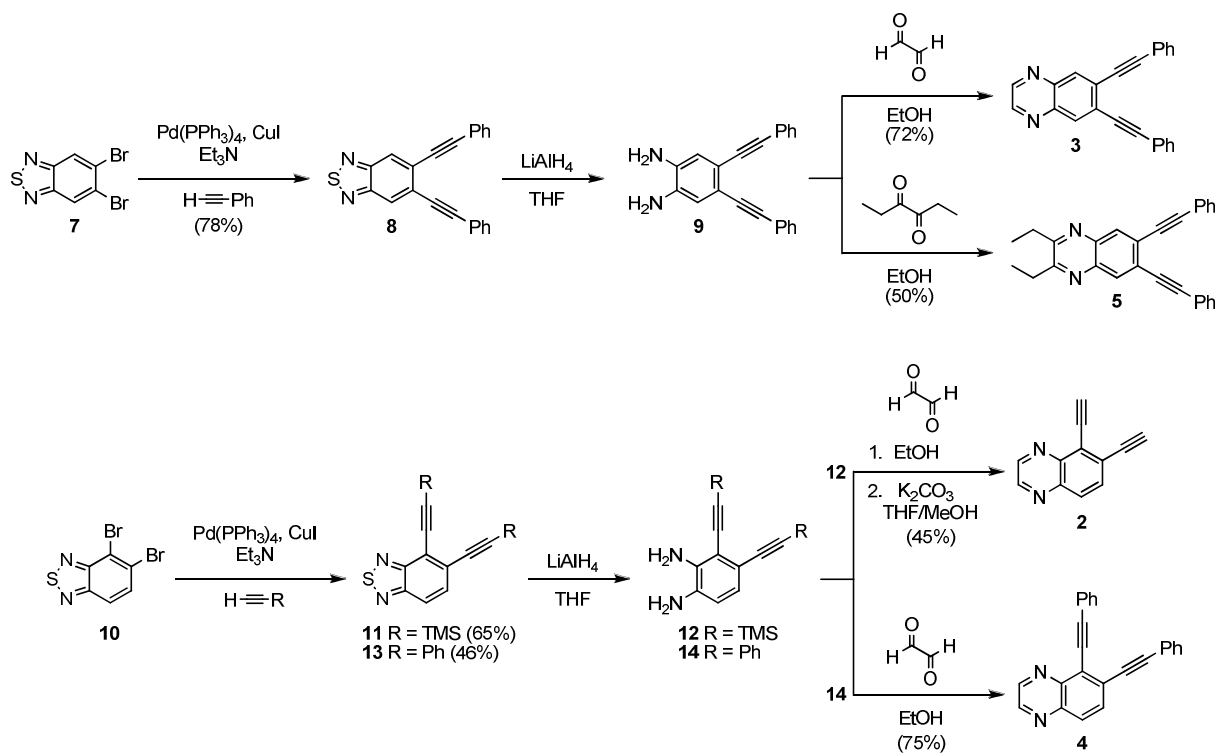
^aData for the nitrogen proximal to the carbon radical are provided in Table S5.

Overall, the data suggests weak interaction between the nitrogen atom and the proximal radical center in the arynes derived from angular quinoxalenediynes **2** and **4** that is more measurable along the C¹–C⁶ versus C¹–C⁵ channel that leads to a small increase in zwitterionic character. These effects, however, impart relatively small changes to the reaction energetics compared to aromatic stabilization energy along the C¹–C⁶ channel for the angular derivatives. Future studies will more systematically examine aromatic stabilization energies and biradical stabilization energies to further refine the role of aromaticity and electronic effect imparted by nitrogen atoms on cyclization of quinoxalenediynes **1–4** that is beyond scope of the current paper.

Syntheses. We previously reported the synthesis and thermal C¹–C⁶ cyclization of 6,7-diethynylquinoxaline **1** starting from 1,2-diiodo-4,5-dinitrobenzene.²⁵ In the present study two alternative synthetic routes were employed to prepare quinoxalenediynes **2–6** to examine kinetics and photochemical reactivity. Linear 6,7-bis(phenylethynyl)quinoxaline derivatives **3** and **5** were prepared in three steps from commercially available 5,6-dibromo-2,1,3-benzothiadiazole **7** as outlined in Scheme 1. Sonogashira coupling³⁸ of **7** with phenylacetylene readily afforded benzothiadiazole **8** in 78% yield. Sulfur extrusion with LiAlH₄ produced diamine **9** and

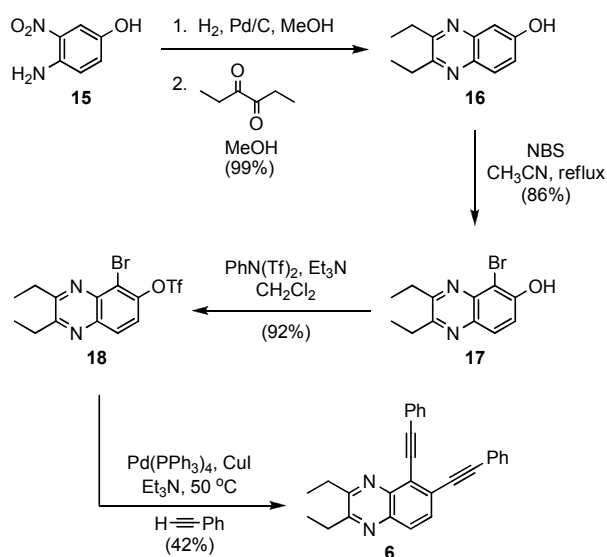
immediate condensation with glyoxal or 3,4-hexanedione in ethanol afforded linear quinoxalenediynes **3** and **5** in two-step yields of 72% and 50%, respectively. An analogous route was employed to generate angular derivatives 5,6-diethynylquinoxaline **2** and 5,6-bis(phenylethynyl)quinoxaline **4** from 4,5-dibromo-2,1,3-benzothiadiazole **10**.³⁹ Sonogashira coupling of **10** with trimethylsilylacetylene gave benzothiadiazole-based enediyne **11** in 65% yield. Subsequent treatment with LiAlH₄ followed by condensation with glyoxal and desilylation produced 5,6-diethynylquinoxaline **2** in a three step 45% yield. Similarly, Sonogashira coupling between phenylacetylene and **10** gave benzothiadiazole-based enediyne **13** in 46%. Finally, treatment of **13** with LiAlH₄ and condensation with glyoxal produced angular quinoxalenediynes **4** in a two-step 75% yield.

Scheme 1. Syntheses of Quinoxalenediynes from Dibromobenzothiadiazoles



Syntheses of quinoxalenediynes from dibromo-2,1,3-benzothiadiazole isomers is our preferred method to introduce alterations to the quinoxaline core as condensation with appropriate 1,2-dicarbonyls is conducted as the final step. In addition, we sought development of an alternative synthetic route that would employ late stage insertion of the enediyne motif more suited to modify alkyne substitution pattern in the future. This was accomplished for preparation of the angular 5,6-diethynylquinoxaline system starting from 4-amino-3-nitrophenol **15** and used to prepare quinoxalenediayne **6** as outlined in Scheme 2. Hydrogenation of **15** followed by condensation with 3,4-hexanedione afforded 2,3-diethyl-6-hydroxyquinoxaline **16** in a two-step 99% yield. Selective bromination of **16** with NBS then afforded 5-bromo-6-hydroxyquinoxaline **17** in 86% yield and treatment with N-phenyltriflimide gave triflate **18** in 92% yield. Finally, Sonogashira coupling of **18** with phenylacetylene provided 2,3-diethyl-5,6-bis(phenylethynyl)quinoxaline **6** in 42% yield.

Scheme 2. Alternative Synthesis of Angular Quinoxalenediayne 6



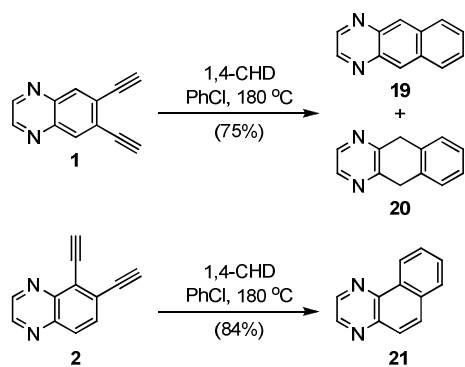
1
2
3 Quinoxalenediynes **1–6** were isolated as stable solids and purified by column
4 chromatography or recrystallization prior to examining reactivity. Terminal quinoxalenediynes **1**
5 and **2** were prepared to conduct kinetic studies while phenyl substituents in derivatives **3–6** were
6 added to promote photochemical reactivity. Ethyl groups present in **5** and **6** were added to
7 facilitate solubility and to prevent the potential for radical reactivity alpha to the ring nitrogen
8 atoms (Minisci reaction⁴⁰).
9
10
11
12
13
14
15
16

17 Electronic absorbance spectra for quinoxalenediynes **3–6** in CH₂Cl₂ were characterized
18 by a strong absorption band between 280–300 nm with one or two lower energy absorbance
19 bands from 360–380 nm. Finally, emission spectra of phenylethynyl quinoxalenediynes **3–6**
20 gave a single broad emission band ranging from 399–449 nm, with larger Stokes shifts observed
21 for angular isomers **4** and **6**.
22
23
24
25
26
27
28

29 Prior to examining reaction kinetics, bulk thermal cyclizations of **1** and **2** were conducted
30 in chlorobenzene at 180 °C containing excess 1,4-cyclohexadiene (Scheme 3). For both terminal
31 diethynylquinoxaline isomers, Bergman cyclization was the only observed reaction channel,
32 supporting our calculations indicating C¹–C⁶ cyclization is the preferred kinetic and
33 thermodynamic pathway. For linear 6,7-diethynylquinoxaline **1**, however, formation of
34 benzo[*g*]quinoxaline **19** was accompanied by slow formation of hydrogenated 5,10-
35 dihydrobenzo[*g*]quinoxaline **20** (combined 75% yield, with pure **19** isolated in 30% yield upon
36 DDQ oxidation of the product mixture).²⁵ In comparison, thermal cyclization of 5,6-
37 diethynylquinoxaline **2** afforded benzo[*f*]quinoxaline **21** in 84% yield with no evidence of the
38 corresponding hydrogenated product forming.
39
40
41
42
43
44
45
46
47
48
49
50
51
52
53
54

55 **Scheme 3. Thermal Cyclization of Quinoxalenediynes 1 and 2**

56
57
58
59
60



Kinetic Studies. Kinetics for **1** and **2** were followed under conditions originally described by Grissom *et al.*⁴¹ and more recently modified by Alabugin *et al.*⁴² (Figure 5). Observed rate constants for the disappearance of quinoxalenediynes and formation of benzoquinoxaline products were monitored as a function of 1,4-cyclohexadiene concentration. As described by Alabugin, monitoring the effect of 1,4-cyclohexadiene concentration on the overall reaction kinetics allows determination of k_1 , the true first order rate constant for cyclization, as well as the k_1/k_2 ratio graphically from equation 2 (assuming k_3 is slow in the presence of excess 1,4-cyclohexadiene and formation of hydrogenated adduct **20** from **19** is minimal).⁴² Deconvolution of rate constants from the measured k_{obs} is ideally suited to examine the effect of extended benzannelation orientation on Bergman cyclization of quinoxalenediynes **1** and **2**. In the case of linear **1**, diluted aromaticity gain predicted computationally should lead to a fast retro-Bergman cyclization, with overall kinetics highly dependent on 1,4-cyclohexadiene concentration and a relatively large k_1/k_2 ratio. In comparison, for angular **2** the gain of a new aromatic sextet will either render Bergman cyclization irreversible, and thus show no dependence on 1,4-cyclohexadiene concentration, or show a weaker dependence on 1,4-cyclohexadiene concentration with a smaller k_1/k_2 ratio (assuming comparable k_2 values for **1** and **2**). As a result, monitoring the effect of 1,4-cyclohexadiene concentration on reaction kinetics for **1** and **2**

can support our computational data and provide experimental insight into the effect of extended benzannelation orientation on Bergman cyclization energetics.

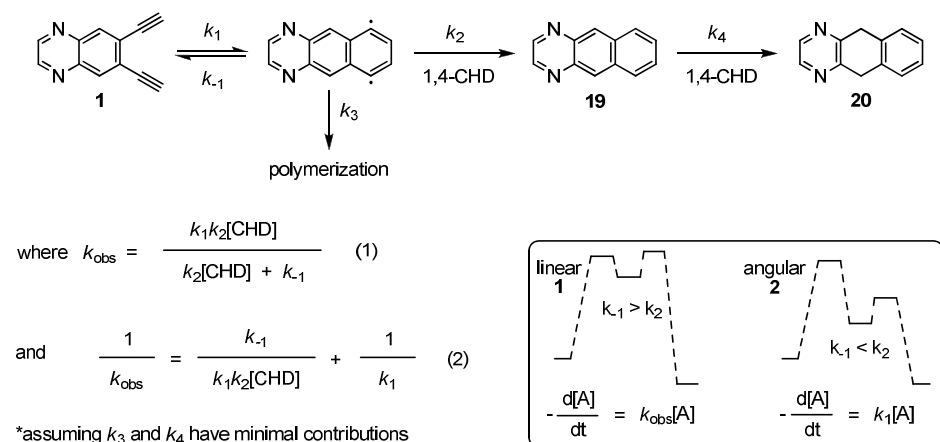


Figure 5. Kinetic model for cyclization of quinoxalenediynes (reference 42).

Kinetic plots monitoring the disappearance of quinoxalenediynes **1** and **2** in the presence of excess 1,4-cyclohexadiene gave good linearity monitored to 2–3 half-lives indicating first order or pseudo-first order decay. Similarly, product formation from **1** showed excellent linearity through the first 1–2 reaction half-lives. However, at longer reaction time, product analysis was complicated by secondary formation of **20** and the kinetic significance of k_4 . As a result, plots of product formation from **1** were only plotted through the first 1–2 half-lives and the small contribution of product **20** was included in the determination of total percent of product at time t .⁴³ Product analysis for **2**, which showed no indication of secondary products via transfer hydrogenation from 1,4-cyclohexadiene, gave good correlation out to 2–3 half-lives.

Observed rate constants for the disappearance of quinoxalenediynes **1** and **2** and formation of benzoquinoxaline products as a function of 1,4-cyclohexadiene concentration at 180 °C are given in Table 8. For linear isomer **1**, formation of benzoquinoxaline products gave a

1
2
3 slower k_{obs} value compared to disappearance of starting quinoxalenediynes at low 1,4-
4
5 cyclohexadiene concentration (50 equivalents or less). This can be explained by significant
6
7 polymerization of the diradical intermediate with k_3 becoming a kinetically significant step. At
8
9 higher 1,4-cyclohexadiene concentrations (100–250 equivalents) both the disappearance of
10
11 quinoxalenediynes **1** and formation of cyclized products **19** and **20** showed a strong dependence
12
13 on 1,4-cyclohexadiene concentration with comparable observed rate constants through the first
14
15 1–2 reaction half-lives. At longer reaction times, however, k_4 becomes significant leading to
16
17 more scatter in the plots of product formation from **1**. Despite this complexity, it is clear that
18
19 6,7-diethynylquinoxaline **1** shows a strong dependence on 1,4-cyclohexadiene concentration,
20
21 indicative of a reversible Bergman cyclization, as the rate of product formation increases 6-fold
22
23 across the range of 1,4-cyclohexadiene concentrations examined. Finally, a plot of $1/k_{\text{obs}}$ versus
24
25 $1/[\text{CHD}]^{44}$ for both quinoxalenediynes disappearance ($R^2 = 0.972$) and benzoquinoxaline
26
27 formation ($R^2 = 0.975$) provided an averaged k_1 value of $7.72 \pm 1.4 \times 10^{-4} \text{ (s}^{-1}\text{)}$ and a k_1/k_2 ratio
28
29 of 4.30 ± 0.85 for the cyclization of 6,7-diethynylquinoxaline **1** at 180 °C.
30
31
32
33
34
35
36
37
38

39 **Table 8. Observed Rate Constants for the Disappearance of Quinoxalenediynes and**
40
41 **Formation of Benzoquinoxalines at 180 °C^a**
42

DEQ	[1,4-CHD] M	$k_{\text{obs}} \text{ sm} \times 10^4$	$k_{\text{obs}} \text{ pdt} \times 10^4$	$k_1 \times 10^4$	k_1/k_2
1^b	0.258	0.505 ± 0.03	0.314 ± 0.01	7.72 ± 1.4	4.3 ± 0.9
	0.280	0.528 ± 0.03	0.378 ± 0.02		
	0.553	0.878 ± 0.04	0.860 ± 0.05		
	0.824	1.15 ± 0.03	1.23 ± 0.07		
	0.835	1.34 ± 0.08	1.39 ± 0.08		
	1.10	1.56 ± 0.07	1.60 ± 0.11		
	1.29	1.71 ± 0.05	1.74 ± 0.10		
	1.37	1.80 ± 0.08	1.86 ± 0.15		
2^c	0.280	33.1 ± 1.5	29.8 ± 2.3	29.0 ± 1.2	
	0.410	29.0 ± 1.1	30.2 ± 2.2		
	0.600	28.0 ± 2.0	27.8 ± 1.7		

^aPseudo-first order rate constants (s^{-1}) for **1**. First order rate constants (s^{-1}) for **2**. ^bInitial concentration of **1** = 5.3×10^{-3} M. ^cInitial concentration of **2** = 5.5×10^{-3} M.

Kinetic data for angular quinoxalenediyne **2** again showed a faster rate of starting material disappearance compared to the measured rate of product formation at the lowest 1,4-cyclohexadiene concentration examined (50 equivalents), indicative of polymerization. At higher 1,4-cyclohexadiene concentrations (75–100 equivalents), measured rates for disappearance of quinoxalenediyne **2** and formation of benzoquinoxaline **21** were within experimental error. More importantly, disappearance of quinoxalenediyne **2** and formation of benzoquinoxaline **21** showed no dependence on hydrogen atom donor concentration as the measured rates were in excellent agreement. These results are indicative of an irreversible Bergman cyclization with the measured rate directly providing k_1 . Overall, the averaged k_1 rate constant measured for Bergman cyclization of 5,6-diethynylquinoxaline **2** was $2.90 \pm 0.12 \times 10^{-3}$ (s^{-1}).

The above experimental data supports our calculations and is consistent with previous literature data in a number of ways. First, the observed change in rate determining step from hydrogen atom abstraction for **1** to Bergman cyclization for **2** is consistent with the larger calculated retro-Bergman barrier for **2** (assuming hydrogen atom abstraction for **1** and **2** are comparable). Second, the faster k_1 rate constant measured for **2** compared to **1** supports the lower Bergman cyclization barrier calculated for **2**. Experimentally, at 180 °C k_1 is 3.8 times faster for angular derivative **2** compared to the linear isomer **1** (or $\Delta\Delta H^\ddagger = 1.20$ kcal/mol). Based on our calculations (Tables S6 and S7) at 180 °C, this ratio is predicted to be 2.32:1 (or $\Delta\Delta H^\ddagger = 0.76$ kcal/mol) in favor of **2**, in excellent agreement with the measured values from the kinetic studies. Third, the observed rate of disappearance of **1** at 180 °C in the presence of 100-fold

1
2
3 excess 1,4-cyclohexadiene (8.78×10^{-5}) is significantly slower than the rate of disappearance of
4
5 1,2-diethynylbenzene reported by Alabugin *et al.* under identical conditions (7.83×10^{-4}).⁴²
6
7 Assuming comparable k_2 rates, this result is indicative of a larger k_1 rate constant upon linear
8
9 extended benzannelation present in **1**. Furthermore, the measured k_1/k_2 ratio for
10
11 quinoxalenediynes **1** (4.3) is significantly larger *with k_1 becoming the dominant term* compared to
12
13 k_1/k_2 values measured for 3-nitro-1,2-diethynylbenzene (0.16 at 164 °C) and 4-nitro-1,2-
14
15 diethynylbenzene (0.10 at 170 °C) by Alabugin.⁴² Fourth, though only limited data is available
16
17 to plot equation 2, the rate of thermal Bergman cyclization of 2,3-diethynylnaphthalene shows a
18
19 strong 1,4-cyclohexadiene dependence similar to quinoxalenediynes **1** with a large k_1/k_2 ratio (5.1
20
21 at 152 °C).¹⁶ Finally, gain of a new aromatic sextet may explain earlier Bergman cyclization
22
23 kinetic data reported in the literature including the increased reactivity of cinnolinoenediynes
24
25 compared to analogous benzo-fused enediynes⁴⁵ and the absence of 1,4-cyclohexadiene
26
27 concentration dependence on the rate of cyclization of imidazole-fused enediynes.⁴⁶
28
29
30
31
32
33

34 The combined computational and kinetic data indicates that the retro-Bergman ring
35
36 opening barrier for 6,7-diethynylquinoxaline **1** is extremely low and leads to k_1 becoming faster
37
38 than the rate of hydrogen atom abstraction k_2 . However, retro-Bergman ring opening is
39
40 effectively shut down for the isomeric 5,6-diethynylquinoxaline **2** as the gain of a new aromatic
41
42 sextet decreases Bergman cyclization endothermicity. Though the contribution from the nitrogen
43
44 lone pair remains to be fully dissected, it is evident that extended benzannelation orientation in
45
46 quinoxalenediynes **1** and **2** has a significant influence on Bergman cyclization energetics.
47
48
49

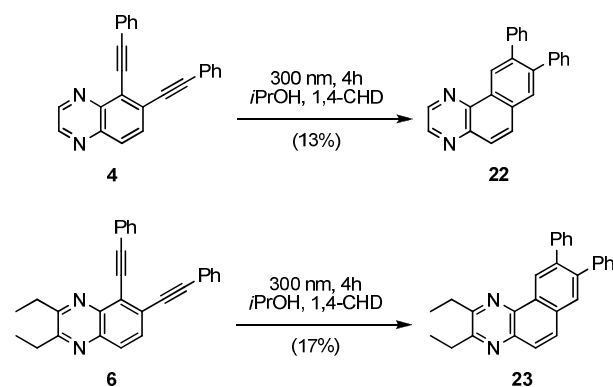
50 **Photochemical Reactivity.** With terminal quinoxalenediynes **1** and **2** readily undergoing
51
52 thermal C¹–C⁶ Bergman cyclization, we turned our attention towards photocyclization of
53
54 phenylethynyl derivatives. Photochemical reactivity of quinoxalenediynes **3–6** was examined in
55
56
57
58
59
60

1
2
3 a Rayonet RPR 100 reactor equipped with sixteen 3000 Å lamps. Initial studies were conducted
4
5 on angular 5,6-bis(phenylethynyl)quinoxaline **4** in isopropanol, the most common solvent used
6
7 in photo-Bergman cyclizations. Under dilute conditions, complete consumption of
8
9 quinoxalenediyne **4** was observed in four hours, providing a low and variable yield (1–5%) of
10
11 C¹–C⁶ cyclization product **22** (Scheme 4). Addition of 1,4-cyclohexadiene led to more
12
13 reproducible yields of benzoquinoxaline **22**, though the highest yield obtained was only
14
15 marginally improved (7%). Optimal yields were obtained upon increasing reaction concentration
16
17 (3 mL isopropanol per mg **4**, 200 equivalents 1,4-cyclohexadiene, 4 h), providing **22** in 13%
18
19 yield (based on 32% recovered quinoxalenediyne **4**). An increase in reaction time gave higher
20
21 conversion of **4**, however, significant polymerization led to lower isolated yields of **22** upon
22
23 extended irradiation. Similarly, attempts to further increase reaction concentration led to poor
24
25 solubility of quinoxalenediyne **4** in isopropanol, while addition of co-solvents (acetonitrile,
26
27 toluene) reduced isolated yields of **22**. Finally, with a significant absorbance band near 360 nm,
28
29 photolysis of quinoxalenediyne **4** under our optimized conditions with 3500 Å lamps provided a
30
31 comparable 10% yield of benzoquinoxaline **22** (based on 21% recovered starting material).
32
33
34
35
36
37

38
39 Rapid consumption of quinoxalenediyne **4** under dilute conditions, along with evidence
40
41 of higher molecular weight adducts observed by GCMS analysis, led us to speculate that radical
42
43 additions alpha to the quinoxaline nitrogen atoms (Minisci reaction⁴⁰) may contribute to rapid
44
45 degradation of starting material. To limit this potential side reaction, ethyl substituents were
46
47 introduced at positions 2 and 3 of the quinoxaline core in **6**. Irradiation of quinoxalenediyne **6**
48
49 under our optimized conditions employed for **4** (3 mL isopropanol per mg **6**, 200 equivalents
50
51 1,4-cyclohexadiene, 300 nm, 4 hours) gave 49% conversion of **6** with 17% yield of
52
53 benzoquinoxaline **23**, a 30% increase in yield compared to **4**. It should be noted, however, that
54
55
56
57
58
59
60

1
2
3 this improved yield was primarily based on increased recovery of starting material as the isolated
4 masses of **22** and **23** were comparable under identical conditions. For comparison, irradiation of
5
6 masses of **22** and **23** were comparable under identical conditions. For comparison, irradiation of
7
8 1,2-bis(phenylethynyl)benzene under our standard conditions afforded 2,3-diphenylnaphthalene
9
10 in 9% yield (based on recovery of 10% unreacted starting material).
11
12
13
14

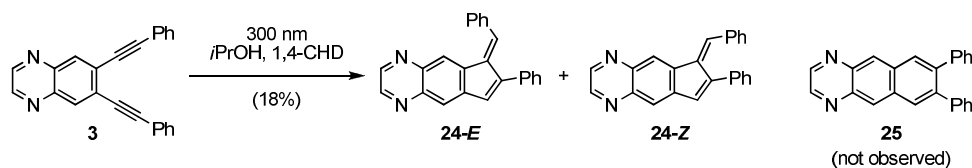
15 **Scheme 4. Photo-Bergman Cyclization of Angular Quinoxalenediynes 4 and 6**



Photocyclization of linear analog **3** at 300 nm under identical conditions, however, gave no evidence of C¹-C⁶ Bergman cyclization product **25**. Alternatively, a 2:1 mixture of C¹-C⁵ fulvene adducts, **24-E** and **24-Z**, was produced in a combined 18% yield (Scheme 5). Confirming the identity of **24-E** and **24-Z**, however, proved challenging as the mixture of fulvene isomers was difficult to completely separate chromatographically. Based on computational modeling, the fulvene exocyclic radical center derived from **3** (i.e. **3-Lin**) is approximately linear, supporting formation of both fulvene isomers. Furthermore, previous studies on fulvene mono-radical geometries formed upon radical cyclization of 1,2-bis(phenylethynyl)benzene derivatives with AIBN/Bu₃SnH were similarly found to afford *E/Z*-fulvene isomers with modest stereoselectivity favoring the *E*-isomer.³² To confirm assignment of **24-E** as the major isomer, computational predictions of ¹H NMR spectra for **24-E** and **24-Z**

were conducted to compare calculated chemical shifts with experimental data. This analysis focused on the four aromatic signals of the quinoxaline core and the two vinyl hydrogens of the newly formed fulvene ring. For the major isomer, the average chemical shift deviation $\Delta\delta$ was 0.13 ppm when compared to the calculated values for **24-E** versus a $\Delta\delta$ value of 0.20 ppm for **24-Z**. Likewise, the minor isomer gave a closer match to the calculated values for **24-Z** ($\Delta\delta = 0.09$ ppm) versus **24-E** ($\Delta\delta = 0.22$ ppm). In support of these assignments, the minor isomer showed long range coupling between vinyl protons in the fulvene ring ($^5J = 1.1$ Hz) consistent with isomer **24-Z**. Furthermore, π - π stacking of the two phenyl substituents in fulvene **24-Z** shifts the phenyl hydrogens upfield (7.15–6.98 ppm) compared to **24-E** (7.61–7.44 ppm) in agreement with calculated chemical shifts (Figure S1). Photolysis of diethyl analog **5** under identical reaction conditions, however, produced limited quantities of C^1 - C^5 products (< 5%) with the bulk of starting material recovered (46%). Furthermore, separation of the fulvene product mixture derived from **5** was not possible and, as a result, full characterization was not pursued.

Scheme 5. Photocyclization of Linear Quinoxalenediynes **3**



The change in photochemical cyclization pathway from C^1 - C^6 for angular quinoxalenediynes **4** and **6** to C^1 - C^5 for linear quinoxalenediynone **3** highlights the remarkable role of extended benzannelation orientation. Calculations on angular derivative **4** indicate a small

1
2
3 kinetic preference for C¹-C⁵ cyclization ($\Delta\Delta H^\ddagger = 2.2$ kcal/mol favoring C¹-C⁵) with a low retro-
4 ring opening barrier ($\Delta H^\ddagger_{\text{retro}} = 7.48$ kcal/mol). However, gain of a new aromatic sextet renders
5 C¹-C⁶ cyclization of quinoxalenediyne **4** the preferred thermodynamic pathway ($\Delta\Delta H_{\text{rxn}} = 11.57$
6 kcal/mol in favor of C¹-C⁶) with a large retro-Bergman ring opening barrier ($\Delta H^\ddagger_{\text{retro}} = 21.25$
7 kcal/mol). Overall, our calculations and kinetic data are in agreement with the observed
8 photochemical reactivity of angular quinoxalenediynes **4** and **6** that produce C¹-C⁶
9 benzoquinoxalines **22** and **23**, respectively. In comparison, calculations on linear derivative **3**
10 indicate a much smaller thermodynamic preference for C¹-C⁶ cyclization ($\Delta\Delta H_{\text{rxn}} = 3.50$
11 kcal/mol) with a lower retro-Bergman ring opening barrier ($\Delta H^\ddagger_{\text{retro}} = 15.65$ kcal/mol) due to
12 reduced aromatic stabilization energy gained in the linearly fused product. Furthermore, kinetic
13 data on linear quinoxalenediyne **1** suggests retro-Bergman ring opening will predominate over
14 hydrogen atom abstraction upon C¹-C⁶ cyclization of **3** and **5**. With no strong C¹-C⁶
15 thermodynamic driving force, coupled with a larger kinetic preference for C¹-C⁵ cyclization
16 ($\Delta\Delta H^\ddagger = 4.86$ kcal/mol favoring C¹-C⁵), photocyclization of linear quinoxalenediyne **3** leads to
17 exclusive formation of C¹-C⁵ fulvenes **24-E** and **24-Z**. While a change in reaction pathway from
18 C¹-C⁶ Bergman to C¹-C⁵ Schreiner-Pascal cyclization has precedence,³⁶ this change is typically
19 the result of increased steric hindrance for enediynes (as well as enyne-allenes⁴⁷) as opposed to
20 reduced aromatic stabilization energy observed in the current model. The exact nature of how
21 C¹-C⁵ products are produced from quinoxalenediyne **3**, however, is unclear. While our
22 calculations indicate direct C¹-C⁵ cyclization is a viable reaction pathway, radical addition
23 reactions can also contribute to formation of fulvenes **24-E** and **24-Z**.^{32,48,49}
24
25
26
27
28
29
30
31
32
33
34
35
36
37
38
39
40
41
42
43
44
45
46
47
48
49
50
51
52

53 The combined computational and experimental data indicate extended benzannelation
54 orientation can readily influence photochemical reactivity of acyclic phenylethynyl enediynes.
55
56
57
58
59
60

1
2
3 With extended angular benzannelation in quinoxalenediynes **4** and **6**, an irreversible C¹–C⁶
4 photo-Bergman cyclization is favored exclusively as a new aromatic sextet is produced. On the
5
6 other extreme, diluted aromaticity gain upon C¹–C⁶ cyclization of quinoxalenediyne **3** possessing
7
8 extended linear benzannelation effectively shuts down photo-Bergman cyclization. As a result,
9
10 alternative reaction pathways, such as C¹–C⁵ cyclization, become feasible for **3** that are not
11
12 observed in photocyclization of **4** and **6**.
13
14
15
16

17 Conclusion

18
19 The above work describes a combined computational and experimental study on 5,6-
20 diethynylquinoxaline and 6,7-diethynylquinoxaline derivatives to examine the effect of angular
21
22 versus linear extended benzannelation on C¹–C⁵ and C¹–C⁶ cyclization channels of enediynes.
23
24
25
26

27 With extended linear benzannelation, 6,7-diethynylquinoxaline **1** has a slower rate of
28 thermal Bergman cyclization compared to 1,2-diethynylbenzene derivatives and angular 5,6-
29 diethynylquinoxaline **2**. This can be rationalized by a lower retro-Bergman ring opening barrier
30
31 for 6,9-benzo[g]quinoxalyne, formed upon C¹–C⁶ cyclization of **1**, as ring opening of this aryne
32
33 intermediate does not suffer from a large loss of aromatic stabilization. As a result, the rate of
34
35 cyclization of **1** is highly dependent upon the concentration of hydrogen atom donor, with the
36
37 rate of retro-Bergman ring opening four times faster than the rate of hydrogen atom abstraction.
38
39 Calculations support the observed experimental data with increased enthalpy barrier and reaction
40
41 enthalpy for C¹–C⁶ cyclization of **1** compared to **2**. Furthermore, NICS calculations confirm
42
43 decreased aromatic stabilization upon C¹–C⁶ Bergman cyclization of linear quinoxalenediyne **1**
44
45 compared to **2**. Finally, with diluted aromaticity gain and rapid retro-Bergman ring opening,
46
47 photolysis of linear phenylethynyl-substituted quinoxalenediyne **3** leads to C¹–C⁵ Schreiner-
48
49
50
51
52
53
54
55
56
57
58
59
60

1
2
3 Pascal cyclization to fulvene adducts, the kinetically favored pathway based on calculations and
4
5 the primary reaction channel observed.
6
7

8 In contrast, thermal Bergman cyclization of 5,6-diethynylquinoxaline **2**, with extended
9
10 angular benzannelation, is irreversible and the rate independent of hydrogen atom donor
11
12 concentration as observed for simple non-benzannelated enediynes. NICS calculations support
13
14 increased gain in aromatic stabilization energy in the angular 7,10-benzo[*f*]quinoxalyne
15
16 intermediate as the primary factor to rationalize the decreased cyclization endothermicity and
17
18 increased retro-Bergman ring opening barrier calculated for **2**. Finally, with restored aromatic
19
20 stabilization, phenylethynyl-substituted quinoxalenediynes **4** and **6** show modest improvement in
21
22 C¹–C⁶ photo-Bergman cyclization yields compared to 1,2-bis(phenylethynyl)benzene.
23
24
25
26

27 Calculated singlet–triplet splittings and biradical stabilization energies indicate increased
28
29 interaction between the proximal nitrogen atom and the radical center in the aryne intermediate
30
31 derived from angular quinoxalenediynes **2** and **4**. While this may play a small role on overall
32
33 reaction energetics, studies to further define the role of the nitrogen atom on cyclization channels
34
35 of quinoxalenediynes and related naphthalenediynes are under investigation.
36
37
38

39 These results suggest a modification to the current model used to predict kinetics of
40
41 Bergman cyclization, which simply states that benzannelation alters the rate limiting step, to the
42
43 following; generation of a new aromatic sextet renders C¹–C⁶ Bergman cyclization of enediynes
44
45 irreversible. This new model may be equally applied to simple cyclic and acyclic enediynes,
46
47 benzannelated enediynes, heteroaromatic enediynes, enediynes fused to non-benzenoid aromatic
48
49 rings and enediynes fused to extended aromatic systems.
50
51
52

53 Finally, the contrasting photochemical reactivity of linear quinoxalenediynes **3** compared
54
55 to angular quinoxalenediynes **4** and **6** provides an interesting example wherein a change in
56
57
58
59
60

1
2
3 reaction pathway occurs due to energetic considerations of the aryne intermediates as opposed to
4
5 steric considerations of the enediyne reactant. With the majority of photoactivated enediynes
6
7 described in the literature derived from simple benzannelated enediynes, altering the extent and
8
9 orientation of benzannelation may provide a route to design more efficient acyclic enediynes for
10
11 photo-Bergman cyclization.
12
13

14 15 **Experimental Section**

16
17 **Computational Methodology.** All calculations were carried out with the Gaussian 09
18
19 quantum chemistry program.⁵⁰ The mPW1PW91 functional^{51,52} has been shown to accurately
20
21 reproduce crystal structures of arenediynes²³ as well as C¹-C⁶ activation and reaction enthalpies
22
23 for parent compounds (*Z*)-hex-3-ene-1,5-diyne and 1,2-diethynylbenzene,²⁵ and was therefore
24
25 used for the calculations involving quinoxalenediynes **1–4**. Geometry optimizations utilized the
26
27 6-31G(d,p) basis set, and single-point energies for all stationary points utilized the cc-pVTZ
28
29 basis set. Calculations were carried out in the gas phase as reaction energetics for Bergman
30
31 cyclization are not significantly affected by the inclusion of solvation energies.²⁵ Restricted
32
33 wave functions were utilized for the close-shell reactant quinoxalenediynes. Calculations for the
34
35 cyclization transition states and diradical products were carried out with broken-symmetry
36
37 unrestricted wave functions due to the open-shell character of these species.^{3a,12a} Vibrational
38
39 frequency calculations enabled verification of the stationary points as well as tabulation of zero-
40
41 point energy, thermal enthalpy, and thermal entropy corrections, enabling reaction enthalpies and
42
43 reaction free energies to be calculated. Singlet and triplet states were calculated for the transition
44
45 states and diradical products. As all singlet states proved to be lower in energy than the triplet
46
47 states (Table S2), singlet states are used as the focus of the results and discussion.
48
49
50
51
52
53
54
55
56
57
58
59
60

1
2
3
4 Nucleus-independent chemical shifts (NICS) were used to measure the aromaticity of the
5 newly formed rings in the singlet transition states and singlet products of the cyclization
6 reactions.⁵³ The NICS values are calculated at the geometric center of the rings, as determined
7 by averaging the Cartesian coordinates of the carbon atoms comprising the ring. NICS-1 values
8 were also calculated, in which the NICS position was exactly 1 Å above the center of the ring
9 plane.^{13a,54} The NICS-1 values are affected mainly by π contributions, with minimal
10 contributions from the C-C and C-H σ bonds. The NICS calculations used the geometries
11 optimized with the mPW1PW91 functional and the 6-31G(d,p) basis set and are calculated using
12 the same functional with the larger 6-311++G(d,p) basis set needed for accurate NMR
13 calculations.⁵⁵

14
15
16
17
18
19
20
21
22
23
24
25
26
27 Biradical stabilization energies (BSE) are calculated via isodesmic reactions for the
28 hydrogen transfer to the singlet diradical from the corresponding closed-shell species to give a
29 pair of monoradicals. BSE calculations are carried out at the same level of theory used for the
30 cyclization reaction energetics. The enthalpy changes (including zero-point energy and thermal
31 enthalpy corrections) for the isodesmic reactions represent the BSE values for the singlet
32 diradicals. Positive BSEs are indicative of stabilization, while negative BSEs imply
33 destabilization, between two radical sites in the same molecule.

34
35
36
37
38
39
40
41
42
43
44
45
46
47
48
49
50
51
52
53
54
55
56
57
58
59
60

^1H and ^{13}C chemical shifts were calculated using density functional theory methods according to the procedure from Wiitala et al.⁵⁶ Specifically, geometries were first optimized at the B3LYP/6-31G(d) level with chloroform as the solvent (IEF-PCM solvation method). NMR chemical shifts were then calculated in chloroform solvent at the B3LYP/6-311+G(2d,p) level. Chemical shifts relative to TMS were then corrected according to the linear regression formulae given by Wiitala et al (^1H : actual = 0.9333*calculated + 0.1203; ^{13}C : actual = 0.9488*calculated

1
2
3 -2.1134), who developed this method for application to chemical shifts calculated in chloroform
4 solvent in order to correct for systematic errors in the calculated chemical shift values. Relative
5 enthalpies and free energies for the C¹-C⁵ product isomers from cyclization of **3** and **4** (Tables
6 S8 and S9) were computed from the single point energies obtained in chloroform solvent at the
7 B3LYP/6-311+G(2d,p) level and include zero-point energy, thermal enthalpy, and thermal
8 entropy corrections.
9
10
11
12
13
14
15
16

17 **General Procedures.** All reagents and solvents were obtained from commercial
18 suppliers and used without further purification. 6,7-diethynylquinoxaline **1**,²⁵
19 benzo[g]quinoxaline **19**,²⁵ and 4,5-dibromo-2,1,3-benzothiadiazole **10**³⁹ were prepared as
20 previously described. Air sensitive reactions were performed under an inert atmosphere of
21 argon. TLC was performed on precoated silica plates and visualized with short- and long-
22 wavelength UV light. Flash chromatography was conducted with 230–400 mesh silica gel
23 packed in glass columns with the indicated solvent system. Thermolysis reactions were
24 conducted in an oil bath equipped with a temperature controller. Photochemical reactions were
25 conducted in a quartz vessel with a Rayonet photochemical reactor equipped with sixteen 300
26 nm or 350 nm lamps. Melting points were determined in open capillary tubes on a Mel-Temp
27 apparatus and are uncorrected. ¹H and ¹³C NMR spectra were recorded on a 500 MHz
28 spectrometer and are reported in ppm relative to tetramethylsilane (0.0 ppm) for ¹H or CDCl₃
29 (77.0 ppm) for ¹³C. FTIR spectra were obtained as a thin film with a diamond ATR accessory.
30 UV-visible absorbance and emission spectra were obtained on air-equilibrated CH₂Cl₂ solutions
31 at 20–25 °C. Mass spectra were recorded using electrospray ionization with a time-of-flight or
32 Fourier transform ion cyclotron resonance mass analyzer.
33
34
35
36
37
38
39
40
41
42
43
44
45
46
47
48
49
50
51
52
53
54
55
56
57
58
59
60

Kinetic Studies. Separate stock solutions of quinoxalenediyne **1** (10.6 mM) and **2** (11.0 mM) in chlorobenzene were prepared in 5 mL volumetric flasks containing naphthalene (10 mM) as an internal standard. 1.0 mL aliquots of these stock solutions were transferred to 2.0 mL volumetric flasks which contained 50–250 molar equivalents of 1,4-cyclohexadiene. The volumetric flasks were filled to the mark to deliver final solutions that were 5.0 mM naphthalene internal standard, 0.258–1.37 M 1,4-cyclohexadiene, and 5.3 mM quinoxalenediyne **1** or 5.5 mM quinoxalenediyne **2**. 50 μ L of the new 1,4-cyclohexadiene stock solutions were transferred to 10–15 capillary melting point tubes that were frozen in liquid nitrogen and flame sealed leaving enough head space for liquid expansion to fill the capillary tube upon heating. The capillary tubes were then placed on a wire mesh submerged in a pre-heated oil bath at 180 ± 1 °C and monitored out to 2–3 half-lives. Samples were removed at regular time intervals, immediately cooled in an ice-water bath, and analyzed by GC-FID. The GC used the following temperature ramp: initial temperature 100 °C for 2 minutes, ramp 15 °C per minute to 250 °C and hold for 10 minutes; retention time naphthalene internal standard = 1.2 minutes, quinoxalenediyne **1** = 5.0 minutes, benzo[g]quinoxaline **19** = 6.4 minutes, 5,10-dihydrobenzo[g]quinoxaline **20** = 5.6 minutes, quinoxalenediyne **2** = 5.3 minutes, and benzo[f]quinoxaline **21** = 5.9 minutes. The percent starting material and product, relative to internal standard, were determined from area counts. For quinoxalenediyne **1**, two products are produced (benzo[g]quinoxaline **19** and dihydrobenzo[g]quinoxaline **20**) and the percent of each product was determined with the sum of the two products used in the kinetic plots which leads to more scatter in the plots of product formation from quinoxalenediyne **1** at longer time. Each sample was analyzed by GC a minimum of three times to provide relative standard deviations of 5% or less for the averaged percent starting material remaining and percent product formed. For starting material

1
2
3 disappearance, a plot of $\ln(A/A_0)$ versus time provided k_{obs} where A_0 is the initial percent of
4 starting material relative to naphthalene internal standard and A is the percent of starting material
5 at time t . For product formation, a plot of $\ln(P_{\infty}/(P_{\infty}-P))$ versus time provided k_{obs} where P_{∞} is the
6 final percent of product relative to naphthalene internal standard and P is the percent of product
7 at time t (Figures S5 and S7 for quinoxalenediynes **1** and **2**, respectively). Errors in the
8 measured k_{obs} values are standard deviations of the line fits with 95% confidence limits. For
9 quinoxalenediyne **1**, a plot of $1/k_{\text{obs}}$ versus $1/[\text{CHD}]$ provided k_1 and the k_1/k_2 ratio (Figure S6).

10
11
12
13
14
15
16
17
18
19
20 **5,6-bis(phenylethynyl)benzo[*c*][1,2,5]thiadiazole (8).** To an argon degassed solution of
21 **7** (1.50 g, 5.10 mmol) in 1:1 THF/Et₃N (60 mL) was added copper iodide (0.039 g, 0.205 mmol),
22 phenylacetylene (1.56 g, 15.3 mmol) and tetrakis (triphenylphosphine)palladium(0) (0.236 g,
23 0.204 mmol) and the resulting solution was stirred under argon in the dark for 5 hours at 50 °C.
24 Upon completion the reaction mixture was diluted with CH₂Cl₂, washed with saturated aqueous
25 NH₄Cl, saturated aqueous NaCl, dried (Na₂SO₄) and evaporated in vacuo. The resulting solids
26 were recrystallized (ethanol) to give **8** as a brown solid (1.34 g, 78%): mp 150–151 °C; ¹H NMR
27 (500 MHz, CDCl₃) δ 8.25 (s, 2H), 7.65–7.63 (m, 4H), 7.44–7.38 (m, 6H); ¹³C NMR (125 MHz,
28 CDCl₃) δ 153.9, 131.9, 129.0, 128.5, 126.7, 124.3, 122.7, 96.2, 87.4; IR (ATR) cm⁻¹ 2212, 1597,
29 1495; HRMS (ESI-TOF) *m/z*: [M + H]⁺ Calcd for C₂₂H₁₃N₂S 337.0794; Found 337.0801.

30
31
32
33
34
35
36
37
38
39
40
41
42
43
44 **6,7-bis(phenylethynyl)quinoxaline (3).** To a solution of **8** (0.658 g, 1.96 mmol) in THF
45 (11 mL) at 0 °C was added LiAlH₄ (3.1 mL of 2.5 M solution in THF, 7.8 mmol) and the
46 resulting solution allowed to warm to room temperature over 30 minutes. Upon completion the
47 reaction mixture was diluted with wet ether and washed with water, saturated aqueous NH₄Cl,
48 saturated aqueous NaCl, dried (Na₂SO₄) and evaporated in vacuo. The resulting dark red oil was
49 immediately dissolved in ethanol (10 mL), glyoxal (0.291 g of 40% wt/wt solution in water, 2.00
50
51
52
53
54
55
56
57
58
59
60

mmol) was added, and the solution allowed to stir overnight. Upon completion the reaction mixture was concentrated in vacuo and purified by recrystallization (ethanol) to afford **3** as a tan solid (0.468 g, 72%): mp 140–141 °C; ¹H NMR (500 MHz, CDCl₃) δ 8.85 (s, 2H), 8.31 (s, 2H), 7.67–7.64 (m, 4H), 7.44–7.38 (m, 6H); ¹³C NMR (125 MHz, CDCl₃) δ 145.8, 142.4, 132.6, 131.9, 129.0, 128.5, 127.2, 122.7, 95.9, 87.4; IR (ATR) cm⁻¹ 2220, 1604, 1501; UV-vis (CH₂Cl₂) λ_{max} (nm) (log ε) 300 (4.77), 366 (4.08), 384 (4.04); Em (CH₂Cl₂; excitation 350 nm) λ_{max} (nm) 409; HRMS (ESI-TOF) *m/z*: [M + H]⁺ Calcd for C₂₄H₁₅N₂ 331.1230; Found 331.1232.

2,3-diethyl-6,7-bis(phenylethynyl)quinoxaline (5). To a solution of **8** (0.646 g, 1.92 mmol) in THF (11 mL) at 0 °C was added LiAlH₄ (3.1 mL of 2.5 M solution in THF, 7.78 mmol) and the resulting solution allowed to warm to room temperature over 30 minutes. Upon completion the reaction mixture was diluted with wet ether and washed with water, saturated aqueous NH₄Cl, saturated aqueous NaCl, dried (Na₂SO₄) and evaporated in vacuo. The resulting dark red oil was immediately dissolved in ethanol (10 mL), 3,4-hexanedione (0.219 g, 1.92 mmol) was added, and the solution allowed to stir overnight. Upon completion the reaction mixture was concentrated in vacuo and purified by recrystallization (ethanol) to afford **5** as a tan solid (0.372 g, 50%): mp 169–171 °C; ¹H NMR (500 MHz, CDCl₃) δ 8.23 (s, 2H), 7.65–7.63 (m, 4H), 7.40–7.39 (m, 6H), 3.07 (q, *J* = 7.5 Hz, 4H), 1.45 (t, *J* = 7.4 Hz, 6H); ¹³C NMR (125 MHz, CDCl₃) δ 158.4, 140.4, 132.0, 131.8, 128.7, 128.4, 125.6, 123.1, 94.6, 87.9, 28.4, 12.1; IR (ATR) cm⁻¹ 2209, 1609, 1493; UV-vis (CH₂Cl₂) λ_{max} (nm) (log ε) 298 (4.80), 365 (4.08), 379 (4.09); Em (CH₂Cl₂; excitation 350 nm) λ_{max} (nm) 399; HRMS (ESI-TOF) *m/z*: [M + H]⁺ Calcd for C₂₈H₂₃N₂ 387.1856; Found 387.1858.

4,5-bis((trimethylsilyl)ethynyl)benzo[*c*][1,2,5]thiadiazole (11). To an argon degassed solution of **10** (0.530 g, 1.80 mmol) in 1:1 THF/Et₃N (40 mL) was added copper iodide (0.013 g,

0.068 mmol), trimethylsilylacetylene (0.534 g, 5.44 mmol) and tetrakis (triphenylphosphine)palladium(0) (0.082 g, 0.071 mmol) and the resulting solution was stirred under argon in the dark for 8 hours at 50 °C. Upon completion the reaction mixture was diluted with CH₂Cl₂, washed with saturated aqueous NH₄Cl, saturated aqueous NaCl, dried (Na₂SO₄) and evaporated in vacuo. The resulting solids were recrystallized (methanol) to give **11** as a yellow solid (0.382 g, 65%): mp 68–70 °C; ¹H NMR (500 MHz, CDCl₃) δ 7.87 (d, *J* = 9.1 Hz, 1H), 7.62 (d, *J* = 9.1 Hz, 1H), 0.36 (s, 9H), 0.32 (s, 9H); ¹³C NMR (125 MHz, CDCl₃) δ 154.5, 153.8, 132.8, 127.8, 121.1, 119.5, 106.9, 103.9, 102.7, 99.0, 0.04, -0.09; IR (ATR) cm⁻¹ 2144, 1579, 1512; HRMS (ESI-FTICR) *m/z*: [M + H]⁺ Calcd for C₁₆H₂₁N₂SSi₂ 329.0959; Found 329.0959.

5,6-diethynylquinoxaline (2). To a solution of **11** (0.364 g, 1.11 mmol) in THF (8 mL) at 0 °C was added LiAlH₄ (1.4 mL of 2.5 M solution in THF, 3.5 mmol) and the resulting solution allowed to warm to room temperature over 30 minutes. Upon completion the reaction mixture was diluted with wet ether and washed with water, saturated aqueous NH₄Cl, saturated aqueous NaCl, dried (Na₂SO₄) and evaporated in vacuo. The resulting dark red oil was immediately dissolved in ethanol (10 mL), glyoxal (0.272 g of 40% wt/wt solution in water, 1.88 mmol) was added, and the solution allowed to stir overnight. Upon completion the reaction mixture was concentrated in vacuo, dissolved in THF (10 mL) and a saturated solution of K₂CO₃ in methanol (2 mL) was added. Upon stirring 1 hour, the reaction mixture was concentrated in vacuo and purified by flash column chromatography (9:1 dichloromethane/ethyl acetate) to afford **2** as a brown solid (0.089 g, 45%): mp 166–168 °C (d); ¹H NMR (500 MHz, CDCl₃) δ 9.00 (d, *J* = 1.8 Hz, 1H), 8.89 (d, *J* = 1.8 Hz, 1H), 8.07 (d, *J* = 8.8 Hz, 1H), 7.85 (d, *J* = 8.8 Hz, 1H), 3.91 (s, 1H), 3.62 (s, 1H); ¹³C NMR (125 MHz, CDCl₃) δ 146.0, 145.7, 143.4, 142.6, 132.9,

1
2
3 130.1, 128.1, 125.7, 88.4, 84.8, 81.5, 78.7; IR (ATR) cm^{-1} 3222, 2098, 1595, 1490; UV-vis
4
5 (CH₂Cl₂) λ_{max} (nm) (log ϵ) 258 (4.49), 262 (4.52), 330 (3.76); Em (CH₂Cl₂; excitation 350 nm)
6
7
8 λ_{max} (nm) 428; HRMS (ESI-FTICR) m/z : [M + H]⁺ Calcd for C₁₂H₇N₂ 179.0604; Found
9
10 179.0604.
11

12
13 **4,5-bis(phenylethynyl)benzo[*c*][1,2,5]thiadiazole (13).** To an argon degassed solution
14
15 of **10** (1.00 g, 3.40 mmol) in 1:1 THF/Et₃N (60 mL) was added copper iodide (0.026 g, 0.137
16
17 mmol), phenylacetylene (1.04 g, 10.2 mmol) and tetrakis (triphenylphosphine)palladium(0)
18
19 (0.157 g, 0.136 mmol) and the resulting solution was stirred under argon in the dark for 5 hours
20
21 at 50 °C. Upon completion the reaction mixture was diluted with CH₂Cl₂, washed with saturated
22
23 aqueous NH₄Cl, saturated aqueous NaCl, dried (Na₂SO₄) and evaporated in vacuo. The resulting
24
25 solids were purified by flash column chromatography (9:1 hexanes/ethyl acetate) to give **13** as a
26
27 yellow solid (0.521 g, 46%): mp 125–126 °C; ¹H NMR (500 MHz, CDCl₃) δ 7.96 (d, J = 9.1 Hz,
28
29 1H), 7.76 (d, J = 9.1 Hz, 1H), 7.75–7.74 (m, 2H), 7.67–7.65 (m, 2H), 7.45–7.40 (m, 6H); ¹³C
30
31 NMR (125 MHz, CDCl₃) δ 154.6, 154.0, 132.6, 132.1, 131.9, 129.2, 129.1, 128.6, 128.5, 127.4,
32
33 122.8, 122.7, 120.9, 119.4, 100.8, 98.0, 88.2, 84.9; IR (ATR) cm^{-1} 2256, 1587, 1497; HRMS
34
35 (ESI-TOF) m/z : [M + H]⁺ Calcd for C₂₂H₁₃N₂S 337.0794; Found 337.0789.
36
37
38
39

40
41
42 **5,6-bis(phenylethynyl)quinoxaline (4).** To a solution of **13** (0.300 g, 0.892 mmol) in
43
44 THF (10 mL) at 0 °C was added LiAlH₄ (1.4 mL of 2.5 M solution in THF, 3.50 mmol) and the
45
46 resulting solution allowed to warm to room temperature over 30 minutes. Upon completion the
47
48 reaction mixture was diluted with wet ether and washed with water, saturated aqueous NH₄Cl,
49
50 saturated aqueous NaCl, dried (Na₂SO₄) and evaporated in vacuo. The resulting dark red oil was
51
52 immediately dissolved in ethanol (10 mL), glyoxal (0.145 g of 40% wt/wt solution in water, 1.00
53
54 mmol) was added, and the solution allowed to stir overnight. Upon completion the reaction
55
56
57
58
59
60

1
2
3 mixture was concentrated in vacuo and purified by recrystallization (ethanol) to afford **4** as a
4
5 yellow solid (0.220 g, 75%): mp 145–146 °C; ¹H NMR (500 MHz, CDCl₃) δ 9.01 (d, *J* = 1.8 Hz,
6
7 1H), 8.88 (d, *J* = 1.8 Hz, 1H), 8.06 (d, *J* = 8.8 Hz, 1H), 7.93 (d, *J* = 8.7 Hz, 1H), 7.77–7.75 (m,
8
9 2H), 7.66–7.64 (m, 2H), 7.41–7.39 (m, 6H); ¹³C NMR (125 MHz, CDCl₃) δ 145.8, 145.2, 143.3,
10
11 142.6, 132.7, 132.1, 131.9, 129.2, 129.1, 128.9, 128.6, 128.5, 128.4, 126.2, 123.2, 122.8, 101.1,
12
13 97.3, 88.4, 85.6; IR (ATR) cm⁻¹ 2206, 1609, 1499; UV-vis (CH₂Cl₂) λ_{max} (nm) (log ε) 282
14
15 (4.63), 287 (4.63), 364 (4.21); Em (CH₂Cl₂; excitation 350 nm) λ_{max} (nm) 449; HRMS (ESI-
16
17 TOF) *m/z*: [M + H]⁺ Calcd for C₂₄H₁₅N₂ 331.1230; Found 331.1230.

18
19
20
21
22
23 **2,3-diethylquinoxalin-6-ol (16)**. To a solution of 4-amino-3-nitrophenol **15** (2.51 g, 16.3
24
25 mmol) in methanol (125 mL) was added 5% palladium on carbon (0.518 g) and the mixture was
26
27 stirred under an atmosphere of hydrogen in the dark overnight. Upon completion as judged by
28
29 TLC, the reaction mixture was filtered through Celite, degassed with argon, and 3,4-hexanedione
30
31 (1.86 g, 16.3 mmol) was added. After stirring in the dark overnight the solution was
32
33 concentrated in vacuo to afford **16** as a dark brown solid pure by ¹H NMR (3.25 g, 99%): mp
34
35 165–167 °C; ¹H NMR (500 MHz, CDCl₃) δ 9.91 (br s, 1H), 7.64 (d, *J* = 9.1 Hz, 1H), 7.19 (d, *J* =
36
37 2.6 Hz, 1H), 6.95 (dd, *J* = 9.1, 2.6 Hz, 1H); 3.04 (q, *J* = 7.5 Hz, 2H), 2.98 (q, *J* = 7.6 Hz, 2H),
38
39 1.46 (t, *J* = 7.5 Hz, 3H), 1.36 (t, *J* = 7.6 Hz, 3H); ¹³C NMR (125 MHz, CDCl₃) δ 157.5, 156.7,
40
41 154.10, 140.9, 136.4, 129.8, 121.0, 107.9, 28.1, 28.0, 13.1, 13.0; IR (ATR) cm⁻¹ 3082 (br OH),
42
43 1620, 1457; HRMS (ESI-TOF) *m/z*: [M + H]⁺ Calcd for C₁₂H₁₅N₂O 203.1179; Found 203.1176.

44
45
46
47
48
49 **5-bromo-2,3-diethylquinoxalin-6-ol (17)**. To a suspension of **16** (0.752 g, 3.72 mmol)
50
51 in acetonitrile (15 mL) was added N-bromosuccinimide (0.662 g, 3.72 mmol) and the resulting
52
53 solution was refluxed for 30 minutes. An additional portion of N-bromosuccinimide (0.166 g,
54
55 0.933 mmol) was added and the solution refluxed an additional 30 minutes. Upon completion as
56
57
58
59
60

1
2
3 judged by TLC, the reaction mixture was cooled to room temperature, poured onto ice, and
4
5 vacuum filtered to afford **17** as a brown solid pure by ^1H NMR (0.895 g, 86%): mp 126–128 °C;
6
7
8 ^1H NMR (500 MHz, CDCl_3) δ 7.89 (d, $J = 9.1$ Hz, 1H), 7.44 (d, $J = 9.1$ Hz, 1H), 6.20 (s, 1H);
9
10 3.08 (q, $J = 7.4$ Hz, 2H), 3.03 (q, $J = 7.5$ Hz, 2H), 1.47 (t, $J = 7.4$ Hz, 3H), 1.39 (t, $J = 7.5$ Hz,
11
12 3H); ^{13}C NMR (125 MHz, CDCl_3) δ 158.0, 155.2, 153.1, 139.1, 137.2, 128.9, 119.3, 106.7, 28.2,
13
14 27.8, 12.5, 12.0; IR (ATR) cm^{-1} 2583 (br OH), 1613, 1448; HRMS (ESI-TOF) m/z : $[\text{M} + \text{H}]^+$
15
16 Calcd for $\text{C}_{12}\text{H}_{14}\text{BrN}_2\text{O}$ 281.0284; Found 281.0289.
17
18

19
20 **5-bromo-2,3-diethylquinoxalin-6-yl trifluoromethanesulfonate (18).** To a suspension
21
22 of **17** (0.558 g, 1.99 mmol) in CH_2Cl_2 (10 mL) was added Et_3N (1.22 g, 12.1 mmol) and the
23
24 resulting suspension was cooled to 0 °C. $\text{PhN}(\text{Tf})_2$ (0.745 g, 2.09 mmol) was added and the
25
26 solution stirred at 0 °C for 1 hour. Upon completion as judged by TLC, the reaction mixture was
27
28 diluted with CH_2Cl_2 , washed with water, saturated aqueous NaHCO_3 , saturated aqueous NaCl ,
29
30 dried (Na_2SO_4) and evaporated in vacuo. The resulting solids were purified by flash column
31
32 chromatography (7:3 dichloromethane/hexanes) to give **18** as a light yellow solid (0.753 g,
33
34 92%): mp 75–77 °C; ^1H NMR (500 MHz, CDCl_3) δ 8.05 (d, $J = 9.2$ Hz, 1H), 7.61 (d, $J = 9.2$ Hz,
35
36 1H), 3.12–3.05 (m, 4H), 1.49 (t, $J = 7.4$ Hz, 3H), 1.42 (t, $J = 7.5$ Hz, 3H); ^{13}C NMR (125 MHz,
37
38 CDCl_3) δ 159.4, 159.2, 146.8, 140.3, 139.2, 129.4, 122.4, 118.7 (q, $J_{\text{CF}} = 320$ Hz), 118.0, 28.2,
39
40 28.0, 11.8, 11.5; IR (ATR) cm^{-1} 1596, 1422, 1206; HRMS (ESI-TOF) m/z : $[\text{M} + \text{H}]^+$ Calcd for
41
42 $\text{C}_{13}\text{H}_{13}\text{F}_3\text{BrN}_2\text{O}_3\text{S}$ 412.9777; Found 412.9778.
43
44
45
46
47
48

49 **2,3-diethyl-5,6-bis(phenylethynyl)quinoxaline (6).** To an argon degassed solution of
50
51 **18** (0.753 g, 1.82 mmol) in 1:1 THF/ Et_3N (22 mL) was added copper iodide (0.015 g, 0.079
52
53 mmol), phenylacetylene (0.569 g, 5.57 mmol) and tetrakis (triphenylphosphine)palladium(0)
54
55 (0.089 g, 0.077 mmol) and the resulting solution was stirred under argon in the dark for 20 hours
56
57
58
59
60

1
2
3 at 50 °C. GCMS analysis of the crude reaction mixture indicated a significant amount of mono-
4
5 coupled product remained so an additional portion of phenylacetylene (0.186 g, 1.82 mmol) and
6
7 tetrakis (triphenylphosphine)palladium(0) (0.045 g, 0.039 mmol) were added and the solution
8
9 was heated at 50 °C an additional 16 hours. Upon completion as judged by TLC, the reaction
10
11 mixture was diluted with CH₂Cl₂, washed with saturated aqueous NH₄Cl, saturated aqueous
12
13 NaCl, dried (Na₂SO₄) and evaporated in vacuo. The resulting solids were purified by flash
14
15 column chromatography (3:1 chloroform/hexanes) to give **6** as a yellow solid (0.297 g, 42%):
16
17 mp 169–171 °C; ¹H NMR (500 MHz, CDCl₃) δ 7.92 (d, *J* = 8.7 Hz, 1H), 7.78 (d, *J* = 8.6 Hz,
18
19 1H), 7.72–7.70 (m, 2H), 7.66–7.64 (m, 2H), 7.40–7.37 (m, 6H), 3.12 (q, *J* = 7.3 Hz, 2H), 3.06 (q,
20
21 *J* = 7.5 Hz, 2H), 1.56 (t, *J* = 7.3 Hz, 3H), 1.42 (t, *J* = 7.5 Hz, 3H); ¹³C NMR (125 MHz, CDCl₃) δ
22
23 157.9, 141.3, 140.4, 131.9, 131.8, 131.3, 128.7, 128.54, 128.47, 128.4, 126.5, 125.4, 123.8,
24
25 123.2, 100.3, 95.8, 88.8, 86.2, 28.3, 28.2, 12.2, 11.4; IR (ATR) cm⁻¹ 2204, 1595, 1495, 1453;
26
27 UV-vis (CH₂Cl₂) λ_{max} (nm) (log ε) 282 (4.70), 289 (4.73), 364 (4.37); Em (CH₂Cl₂; excitation
28
29 350 nm) λ_{max} (nm) 429; HRMS (ESI-TOF) *m/z*: [M + H]⁺ Calcd for C₂₈H₂₃N₂ 387.1856; Found
30
31 387.1857.

32
33
34
35
36
37
38
39 **Benzo[*f*]quinoxaline (21).** A solution of **2** (0.010 g, 0.056 mmol) in chlorobenzene (16
40
41 mL) and 1,4-cyclohexadiene (1.3 g, 16 mmol) was placed in an Ace pressure tube and sealed.
42
43 The reaction was heated to 180 °C in an oil bath for 2 hours. After cooling to room temperature
44
45 the solution was evaporated in vacuo and the resulting solids were purified by flash column
46
47 chromatography (3:2 hexanes/ethyl acetate) to give **21** as a tan solid (0.0084 g, 84%): mp 56–57
48
49 °C (lit⁵⁷ 55–57 °C); ¹H NMR (500 MHz, CDCl₃) δ 9.25–9.23 (m, 1H), 8.94 (d, *J* = 2.0 Hz, 1H),
50
51 8.92 (d, *J* = 2.0 Hz, 1H), 8.07 (d, *J* = 9.1 Hz, 1H), 7.98–7.96 (m, 2H), 7.81–7.75 (m, 2H); ¹³C
52
53 NMR (125 MHz, CDCl₃) δ 144.4, 143.2, 142.8, 141.8, 133.3, 131.8, 131.0, 129.0, 128.0, 127.7,
54
55
56
57
58
59
60

1
2
3 126.8, 124.5; IR (ATR) cm^{-1} 1602, 1492, 1443; HRMS (ESI-FTICR) m/z : $[\text{M} + \text{H}]^+$ Calcd for
4
5 $\text{C}_{12}\text{H}_9\text{N}_2$ 181.0760; Found 181.0760.
6
7

8 **8,9-diphenylbenzo[*f*]quinoxaline (22)**. To an argon degassed solution of **4** (0.050 g,
9
10 0.151 mmol) in isopropanol (150 mL) in a quartz reaction vessel was added 1,4-cyclohexadiene
11
12 (2.40 g, 30.0 mmol) and the vessel was sealed with a septum. The solution was then irradiated in
13
14 a Rayonet Photochemical Reactor with 16 3000Å lamps for 4 h. The solution was then
15
16 evaporated in vacuo and purified by flash column chromatography (4:1 chloroform/hexanes) to
17
18 give unreacted **4** (0.016 g, 32%) and **22** as a yellow solid (4.3 mg, 13%): mp 197–198 °C; ^1H
19
20 NMR (500 MHz, CD_2Cl_2) δ 9.34 (s, 1H), 9.19 (s, 1H), 8.96 (d, $J = 2.0$ Hz, 1H), 8.32 (s, 2H),
21
22 8.13 (s, 1H), δ 7.37–7.35 (m, 10H); ^{13}C NMR (125 MHz, CDCl_3) δ 144.5, 143.3, 143.0, 142.0,
23
24 141.8, 141.1, 141.0, 140.7, 132.5, 131.5, 130.2, 130.04, 130.00, 129.8, 128.1, 128.0, 127.2,
25
26 127.0, 126.8, 126.4; IR (ATR) cm^{-1} 1597, 1485, 1445; HRMS (ESI-TOF) m/z : $[\text{M} + \text{H}]^+$ Calcd
27
28 for $\text{C}_{24}\text{H}_{17}\text{N}_2$ 333.1386; Found 333.1384.
29
30
31
32
33

34 **2,3-diethyl-8,9-diphenylbenzo[*f*]quinoxaline (23)**. To an argon degassed solution of **6**
35
36 (0.051 g, 0.132 mmol) in isopropanol (150 mL) in a quartz reaction vessel was added 1,4-
37
38 cyclohexadiene (2.40 g, 30.0 mmol) and the vessel was sealed with a septum. The solution was
39
40 then irradiated in a Rayonet Photochemical Reactor with 16 3000Å lamps for 4 h. The solution
41
42 was then evaporated in vacuo and purified by flash column chromatography (4:1
43
44 chloroform/hexanes) to give unreacted **6** (0.026 g, 51%) and **23** as a yellow solid (4.2 mg, 17%):
45
46 mp 140–142 °C; ^1H NMR (500 MHz, CDCl_3) δ 9.28 (s, 1H), 8.00 (d, $J = 9.0$ Hz, 1H), 7.97 (s,
47
48 1H), 7.93 (d, $J = 9.0$ Hz, 1H), 7.34–7.27 (m, 10H), 3.13 (q, $J = 7.5$ Hz, 2H), 3.10 (q, $J = 7.6$ Hz,
49
50 2H), 1.49 (t, $J = 7.5$ Hz, 3H), 1.45 (t, $J = 7.6$ Hz, 3H); ^{13}C NMR (125 MHz, CDCl_3) δ 156.6,
51
52 155.5, 141.6, 141.3, 140.9, 140.3, 140.0, 138.9, 132.2, 130.22, 130.18, 130.0, 129.7, 129.6,
53
54
55
56
57
58
59
60

1
2
3 127.94, 127.92, 127.0, 126.7, 126.6, 126.0, 28.2, 28.1, 12.9, 12.6; IR (ATR) cm^{-1} 1599, 1485,
4
5 1441; HRMS (ESI-FTICR) m/z : $[\text{M} + \text{H}]^+$ Calcd for $\text{C}_{28}\text{H}_{25}\text{N}_2$ 389.2012; Found 389.2011.
6
7

8 **(*E/Z*) 7-phenyl-6-(phenylmethylene)-6*H*-cyclopenta[*g*]quinoxaline (24-*E* and 24-*Z*).**
9

10 To an argon degassed solution of **3** (0.050 g, 0.151 mmol) in isopropanol (150 mL) in a quartz
11 reaction vessel was added 1,4-cyclohexadiene (2.58 g, 32.2 mmol) and the vessel was sealed
12 with a septum. The solution was then irradiated in a Rayonet Photochemical Reactor with 16
13 3000Å lamps for 4 h. The solution was then evaporated in vacuo and purified by flash column
14 chromatography (98:2 chloroform/ethyl acetate) to give unreacted **3** (9.2 mg, 18%) and a 2:1
15 mixture of **24-*E/Z*** as a yellow oil (7.5 mg, 18%). The initial fractions of the separation were
16 further purified by flash chromatography (chloroform to 99:1 chloroform/ethyl acetate) to give a
17 pure sample of major product **24-*E***: ^1H NMR (500 MHz, CDCl_3) δ 8.74 (d, $J = 1.9$ Hz, 1H),
18 8.67 (d, $J = 1.9$ Hz, 1H), 8.20 (s, 1H), 7.88 (s, 1H), 7.61–7.57 (m, 4H), 7.52–7.48 (m, 4H), 7.47–
19 7.44 (m, 2H), 7.43 (s, 1H), 7.11 (s, 1H); ^{13}C NMR (125 MHz, CDCl_3) δ 149.9, 145.3, 144.3,
20 144.0, 143.2, 142.4, 138.5, 138.1, 136.2, 135.2, 135.0, 129.5, 129.2, 129.1, 128.9, 128.8, 128.6,
21 128.2, 123.5, 118.9; HRMS (ESI-FTICR) m/z : $[\text{M} + \text{H}]^+$ Calcd for $\text{C}_{24}\text{H}_{17}\text{N}_2$ 333.1386; Found
22 333.1385. The last fractions of the separation gave an enriched sample of minor product **24-*Z***:
23 ^1H NMR (500 MHz, CDCl_3) δ 8.79 (d, $J = 1.9$ Hz, 1H), 8.77 (d, $J = 1.9$ Hz, 1H), 8.35 (s, 1H),
24 7.96 (s, 1H), 7.92 (s, 1H), 7.19 (d, $J = 1.1$ Hz, 1H), 7.15–7.11 (m, 3H), 7.09–7.05 (m, 5H), 7.01–
25 6.98 (m, 2H); HRMS (ESI-FTICR) m/z : $[\text{M} + \text{H}]^+$ Calcd for $\text{C}_{24}\text{H}_{17}\text{N}_2$ 333.1386; Found
26 333.1385.
27
28
29
30
31
32
33
34
35
36
37
38
39
40
41
42
43
44
45
46
47
48
49
50

51 **Supporting Information**
52

53 Computational details (Tables S1–S10, Figures S1–S4); ^1H and ^{13}C NMR spectra of compounds
54 **2–6, 8, 11, 13, 16–18, 21–24**; electronic absorbance and emission spectra of compounds **1–6**;
55
56
57
58
59
60

1
2
3 kinetic plots for cyclization of **1** and **2** (Figures S5–S7) and Cartesian coordinates for geometry-
4
5 optimized structures. This material is available free of charge via the Internet at
6
7
8 <http://pubs.acs.org>.
9

10 **Acknowledgements**

11
12 Funding for the project has been provided by the Donors of the American Chemical Society
13
14 Petroleum Research Fund (Grant 55293-UR4); the California State University Program in
15
16 Education and Research in Biotechnology (CSUPERB); the California State University,
17
18 Sacramento, Research and Creative Activity (RCA) grant, Instructionally Related Activities
19
20 (IRA) grants and Academically Related Activities (ARA) grants.
21
22
23

24 **References**

- 25
26
27 1. Mohamed, R. K.; Peterson, P. W.; Alabugin, I. V. *Chem. Rev.* **2013**, *113*, 7089.
28
29 2. (a) Jones, R. R.; Bergman, R. G. *J. Am. Chem. Soc.* **1972**, *94*, 660. (b) Bergman, R. G. *Acc.*
30
31 *Chem. Res.* **1973**, *6*, 25.
32
33 3. (a) Prall, M.; Wittkopp, A.; Schreiner, P. R. *J. Phys. Chem. A* **2001**, *105*, 9265. (b) Vavilala,
34
35 C.; Byrne, N.; Kraml, C. M.; Ho, D. M.; Pascal, R. A. *J. Am. Chem. Soc.* **2008**, *130*, 13549.
36
37 4. (a) Myers, A. G.; Kuo, E. Y.; Finney, N. S. *J. Am. Chem. Soc.* **1989**, *111*, 8057. (b) Nagata,
38
39 R.; Yamanaka, H.; Okazaki, E.; Saito, I. *Tetrahedron Lett.* **1989**, *30*, 4995.
40
41 5. Schmittel, M.; Strittmatter, M.; Kiau, S. *Tetrahedron Lett.* **1995**, *36*, 4975.
42
43 6. (a) Galm, U.; Hager, M. H.; Van Lanen, S. G.; Ju, J.; Thorson, J. S.; Shen, B. *Chem. Rev.*
44
45 **2005**, *105*, 739. (b) *Enediayne Antibiotics as Antitumor Agents*; Borders, D. B., Doyle, T. W.,
46
47 Eds.; Marcel Dekker: New York, 1995. (c) *Neocarzinostatin: The Past, Present, and Future of*
48
49 *an Anticancer Drug*; Maeda, H., Edo, K., Ishida, N., Eds.; Springer: New York, 1997.
50
51
52
53
54
55
56
57
58
59
60

- 1
2
3 7. (a) Nicolaou, K.C.; Dai, W-M. *Angew. Chem., Int. Ed.* **1991**, *30*, 1387. (b) Maier, M. E.
4
5 *Synlett* **1995**, 13. (c) Grissom, J.W.; Gunawardena, G. U.; Klingberg, D.; Huang, D.
6
7 *Tetrahedron* **1996**, *52*, 6453. (d) Kar, M; Basak, A. *Chem. Rev.* **2007**, *107*, 2861.
8
9
10 8. (a) Bowles, D. M.; Palmer, G. J.; Landis, C. A.; Scott, J. L.; Anthony, J. E. *Tetrahedron* **2001**,
11
12 *57*, 3753. (b) Raviola, C.; Protti, S.; Ravelli, D.; Fagnoni, M. *Chem. Soc. Rev.* **2016**, *45*, 4364.
13
14
15 9. (a) John, J. A.; Tour, J. M. *J. Am. Chem. Soc.* **1994**, *116*, 5011. (b) Rule, J. D.; Moore, J. S.
16
17 *Macromolecules* **2005**, *38*, 7266. (c) Xiao, Y.; Hu, A. *Macromol. Rapid Commun.* **2011**, *32*,
18
19 1688.
20
21
22 10. Sun, Q.; Zhang, C.; Li, Z.; Kong, H.; Tan, Q.; Hu, A.; Xu, W. *J. Am. Chem. Soc.* **2013**, *135*,
23
24 8448.
25
26
27 11. Halter, R. J.; Fimmen, R. L.; McMahon, R. J.; Peebles, S. A.; Kuczkowski, R. L.; Stanton, J.
28
29 *F. J. Am. Chem. Soc.* **2001**, *123*, 12353.
30
31
32 12. (a) Schreiner, P. R.; Navarro-Vazquez, A.; Prall, M. *Acc. Chem. Res.* **2005**, *38*, 29. (b)
33
34 Sherer, E. C.; Kirschner, K. N.; Pickard, F. C., IV; Rein, C.; Feldgus, S.; Shields, G. C. *J. Phys.*
35
36 *Chem. B* **2008**, *112*, 16917. (c) Kraka, E.; Cremer, D. *WIREs Comput. Mol. Sci.* **2014**, *4*, 285.
37
38
39 13. (a) Stahl, F.; Moran, D.; Schleyer, P. v. R.; Prall, M.; Schreiner, P. R. *J. Org. Chem.* **2002**,
40
41 *67*, 1453. (b) De Proft, F.; Schleyer, P. v. R.; Lenthe, J. H. v.; Stahl, F.; Geerlings, P. *Chem. Eur.*
42
43 *J.* **2002**, *8*, 3402.
44
45
46 14. (a) Roth, W. R.; Hopf, H.; Horn, C. *Chem. Ber.* **1994**, *127*, 1765. (b) Roth, W. R.; Hopf, H.;
47
48 Wasser, T.; Zimmermann, H.; Werner, C. *Liebigs Annal.* **1996**, 1691. (c) Prall, M.; Wittkopp,
49
50 A.; Schreiner, P. R. *J. Phys. Chem. A* **2001**, *105*, 9265.
51
52
53 15. Koseki, S.; Fujimura, Y.; Hiram, M. *J. Phys. Chem. A* **1999**, *103*, 7672.
54
55
56 16. Kaneko, T.; Takahashi, M.; Hiram, M. *Tetrahedron Lett.* **1999**, *40*, 2015.
57
58
59
60

- 1
2
3
4
5
6
7
8
9
10
11
12
13
14
15
16
17
18
19
20
21
22
23
24
25
26
27
28
29
30
31
32
33
34
35
36
37
38
39
40
41
42
43
44
45
46
47
48
49
50
51
52
53
54
55
56
57
58
59
60
17. Lockhart, T. P.; Comita, P. B.; Bergman, R. G. *J. Am. Chem. Soc.* **1981**, *103*, 4082.
18. Choy, N.; Kim, C. S.; Ballesteros, C.; Artigas, L.; Diez, C.; Lichtenberg, F.; Shapiro, J.; Russell, K. C. *Tetrahedron Lett.* **2000**, *41*, 6955.
19. (a) Galbraith, J. M.; Schreiner, P. R.; Harris, N.; Wei, W.; Wittkopp, A.; Shaik, S. *Chem. Eur. J.* **2000**, *6*, 1446. (b) Alabugin, I. V.; Manoharan, M. *J. Phys. Chem. A* **2003**, *107*, 3363.
20. (a) Alabugin, I. V.; Manoharan, M.; Kovalenko, S. V. *Org. Lett.* **2002**, *4*, 1119. (b) Zeidan, T. A.; Manoharan, M.; Alabugin, I. V. *J. Org. Chem.* **2006**, *71*, 954. (c) Zeidan, T. A.; Kovalenko, S. V.; Manoharan, M.; Alabugin, I. V. *J. Org. Chem.* **2006**, *71*, 962. (d) Pickard, F. C., IV; Shepherd, R. L.; Gillis, A. E.; Dunn, M. E.; Feldgus, S.; Kirschner, K. N.; Shields, G. C.; Manoharan, M.; Alabugin, I. V. *J. Phys. Chem. A* **2006**, *110*, 2517.
21. (a) Alabugin, I. V.; Manoharan, M. *J. Am. Chem. Soc.* **2003**, *125*, 4495. (b) Peterson, P. W.; Shevchenko, N.; Breiner, B.; Manoharan, M.; Lufti, F.; Delaune, J.; Kingsley, M.; Kovnir, K.; Alabugin, I. V. *J. Am. Chem. Soc.* **2016**, *138*, 15617.
22. Schmittel, M.; Kiau, S. *Chem. Lett.* **1995**, 953.
23. Korovina, N. V.; Chang, M. L.; Nguyen, T. T.; Fernandez, R.; Walker, H. J.; Olmstead, M. M.; Gherman, B. F.; Spence, J. D. *Org. Lett.* **2011**, *13*, 3660.
24. Lewis, K. D.; Matzger, A. J. *J. Am. Chem. Soc.* **2005**, *127*, 9968.
25. Spence, J. D.; Rios, A. C.; Frost, M. A.; McCutcheon, C. M.; Cox, C. D.; Chavez, S.; Fernandez, R.; Gherman, B. F. *J. Org. Chem.* **2012**, *77*, 10329.
26. (a) Jones, G. B.; Russell, K. C. The Photo-Bergman Cycloaromatization of Enediyne. In *CRC Handbook of Organic Photochemistry and Photobiology*, 2nd ed.; Horspool, W., Lenci, F., Eds.; CRC Press: Boca Raton, FL, 2004; pp 29–1. (b) Alabugin, I. V.; Yang, W.-Y.; Pal, R. Photochemical Bergman Cyclization and Related Photoreactions of Enediyne. In *CRC*

- 1
2
3 *Handbook of Organic Photochemistry and Photobiology*, 3rd ed.; Griesbeck, A., Oelgemoller,
4 M., Ghetti, F., Eds.; CRC Press: Boca Raton, FL, 2012; Vol. 1, pp 549–592.
5
6
7
8 27. (a) Turro, N. J.; Evenzahav, A.; Nicolaou, K. C. *Tetrahedron Lett.* **1994**, *35*, 8089. (b)
9 Evenzahav, A.; Turro, N. J. *J. Am. Chem. Soc.* **1998**, *120*, 1835.
10
11
12 28. Funk, R. L.; Young, E. R. R.; Williams, R. M.; Flanagan, M. F.; Cecil, T. L. *J. Am. Chem.*
13 *Soc.* **1996**, *118*, 3291.
14
15
16
17 29. Jones, G. B.; Wright, J. M.; Plourde II, G.; Purohit, A. D.; Wyatt, J. K.; Hynd, G.; Fouad, F.
18 *J. Am. Chem. Soc.* **2000**, *122*, 9872.
19
20
21
22 30. Kaneko, T.; Takanashi, M.; Hirama, M. *Angew. Chem., Int. Ed.* **1999**, *38*, 1267.
23
24
25 31. Spence, J. D.; Hargrove, A. E.; Crampton, H. L.; Thomas, D. W. *Tetrahedron Lett.* **2007**, *48*,
26 725.
27
28
29 32. Kovalenko, S. V.; Peabody, S.; Manoharan, M.; Clark, R. J.; Alabugin, I. V. *Org. Lett.* **2004**,
30 *6*, 2457.
31
32
33
34 33. (a) Pangamte, H. N.; Lyngdoh, R. H. D. *J. Phys. Chem. A* **2010**, *114*, 2710. (b) Dong, H.;
35 Chen, B Z.; Huang, M. B.; Lindh, R. *J. Comput. Chem.* **2012**, *33*, 537.
36
37
38 34. (a) Hoffmann, R.; Imamura, A.; Hehre, W. J. *J. Am. Chem. Soc.* **1968**, *90*, 1499. (b)
39 Hoffmann, R. *Acc. Chem. Res.* **1971**, *4*, 1.
40
41
42
43 35. Squires, R. R.; Cramer, C. J. *J. Phys. Chem. A* **1998**, *102*, 9072.
44
45
46 36. Alabugin, I. V.; Manoharan, M. *J. Am. Chem. Soc.* **2003**, *125*, 4495.
47
48
49 37. Peterson, P. W.; Mohamed, R. K.; Alabugin, I. V. *Eur. J. Org. Chem.* **2013**, 2505.
50
51 38. (a) Sonogashira, K.; Tohda, Y.; Hagihara, N. *Tetrahedron Lett.* **1975**, 4467. (b) Chinchilla,
52 R.; Najera, C. *Chem. Rev.* **2007**, *107*, 874.
53
54
55 39. Wasik, R.; Winska, P.; Poznanski, J.; Shugar, D. *J. Phys. Chem. B* **2012**, *116*, 7259.
56
57
58
59
60

- 1
2
3
4
5
6
7
8
9
10
11
12
13
14
15
16
17
18
19
20
21
22
23
24
25
26
27
28
29
30
31
32
33
34
35
36
37
38
39
40
41
42
43
44
45
46
47
48
49
50
51
52
53
54
55
56
57
58
59
60
40. Minisci, F.; Vismara, E.; Fontana, F. *Heterocycles* **1989**, *28*, 489.
41. (a) Grissom, J. W.; Calkins, T. L. *J. Org. Chem.* **1993**, *58*, 5422. (b) Grissom, J. W.; Calkins, T. L.; McMillen, H. A.; Jiang, Y. H. *J. Org. Chem.* **1994**, *59*, 5833. (c) Grissom, J. W.; Gunawardena, G. U. *Tetrahedron Lett.* **1995**, *36*, 4951.
42. Zeidan, T. A.; Kovalenko, S. V.; Manoharan, M.; Alabugin, I. V. *J. Org. Chem.* **2006**, *71*, 962.
43. At the highest 1,4-cyclohexadiene concentration studied, **20** contributes approximately 15% of the total product mixture through first reaction half-life.
44. Data points at the lowest 1,4-cyclohexadiene concentration, where polymerization of the diradical intermediate likely occurs, were not included in plots.
45. Vinogradova, O. V.; Balova, I. A.; Popik, V. V. *J. Org. Chem.* **2011**, *76*, 6937.
46. Zhao, Z.; Peng, Y.; Dalley, N. K.; Cannon, J. F.; Peterson, M. A. *Tetrahedron Lett.* **2004**, *45*, 3621.
47. (a) Schmittel, M.; Strittmatter, M.; Kiau, S. *Tetrahedron Lett.* **1995**, *36*, 4975. (b) Schmittel, M.; Keller, M.; Kiau, S.; Strittmatter, M. *Chem. Eur. J.* **1997**, *3*, 807.
48. For a discussion on C¹–C⁵ versus C¹–C⁶ cyclization of enediynes under thermal conditions, see: (a) Lewis, K. D.; Matzger, A. J. *J. Am. Chem. Soc.* **2005**, *127*, 9968. (b) Vavilala, C.; Byrne, N.; Kraml, C. M.; Ho, D. M.; Pascal, R. A. *J. Am. Chem. Soc.* **2008**, *130*, 13549.
49. For additional examples of radical promoted C¹–C⁵ cyclization of enediynes, see: Peabody, S. W.; Breiner, B.; Kovalenko, S. V.; Patil, S.; Alabugin, I. V. *Org. Biomol. Chem.* **2005**, *3*, 218. For related reductive cyclizations, see: (a) Whitlock, H. W.; Sandvick, P. E.; Overman, L. E.; Reichardt, P. B. *J. Org. Chem.* **1969**, *34*, 879. (b) Alabugin, I. V.; Kovalenko, S. V. *J. Am. Chem. Soc.* **2002**, *124*, 9052. (c) Peterson, P. W.; Shevchenko, N.; Breiner, B.; Manoharan, M.;

- 1
2
3
4
5
6
7
8
9
10
11
12
13
14
15
16
17
18
19
20
21
22
23
24
25
26
27
28
29
30
31
32
33
34
35
36
37
38
39
40
41
42
43
44
45
46
47
48
49
50
51
52
53
54
55
56
57
58
59
60
- Lufti, F.; Delaune, J.; Kingsley, M.; Kovnir, K.; Alabugin, I. V. *J. Am. Chem. Soc.* **2016**, *138*, 15617.
50. Frisch, M. J.; Trucks, G. W.; Schlegel, H. B.; Scuseria, G. E.; Robb, M. A.; Cheeseman, J. R.; Scalmani, G.; Barone, V.; Mennucci, B.; Petersson, G. A.; Nakatsuji, H.; Caricato, M.; Li, X.; Hratchian, H. P.; Izmaylov, A. F.; Bloino, J.; Zheng, G.; Sonnenberg, J. L.; Hada, M.; Ehara, M.; Toyota, K.; Fukuda, R.; Hasegawa, J.; Ishida, M.; Nakajima, T.; Honda, Y.; Kitao, O.; Nakai, H.; Vreven, T.; J. A. Montgomery, J.; Peralta, J. E.; Ogliaro, F.; Bearpark, M.; Heyd, J. J.; Brothers, E.; Kudin, K. N.; Staroverov, V. N.; Keith, T.; Kobayashi, R.; Normand, J.; Raghavachari, K.; Rendell, A.; Burant, J. C.; Iyengar, S. S.; Tomasi, J.; Cossi, M.; Rega, N.; Millam, J. M.; Klene, M.; Knox, J. E.; Cross, J. B.; Bakken, V.; Adamo, C.; Jaramillo, J.; Gomperts, R.; Stratmann, R. E.; Yazyev, O.; Austin, A. J.; Cammi, R.; Pomelli, C.; Ochterski, J. W.; Martin, R. L.; Morokuma, K.; Zakrzewski, V. G.; Voth, G. A.; Salvador, P.; Dannenberg, J. J.; Dapprich, S.; Daniels, A. D.; Farkas, O.; Foresman, J. B.; Ortiz, J. V.; Cioslowski, J.; Fox, D. *J. Gaussian 09, Revision C.01*; Gaussian, Inc.: Wallingford, CT, 2010.
51. Adamo, C.; Barone, V. *J. Chem. Phys.* **1998**, *108*, 664.
52. Perdew, J. P.; Chevary, J. A.; Vosko, S. H.; Jackson, K. A.; Pederson, M. R.; Singh, D. J.; Fiolhais, C. *Phys. Rev. B* **1992**, *46*, 6671.
53. Chen, Z.; Wannere, C. S.; Corminboeuf, C.; Puchta, R.; Schleyer, P. v. R. *Chem. Rev.* **2005**, *105*, 3842.
54. (a) Schleyer, P. v. R.; Jiao, H.; Hommes, N. J. R. v. E.; Malkin, V. G.; Malkina, O. L. *J. Am. Chem. Soc.* **1997**, *119*, 12669. (b) Schleyer, P. v. R.; Manoharan, M.; Wang, Z.-X.; Jiao, H.; Puchta, R.; Hommes, N. J. R. v. E. *Org. Lett.* **2001**, *3*, 2465.

- 1
2
3 55. Cramer, C. J. *Essentials of Computational Chemistry: Theories and Models*; 2nd ed.; John
4 Wiley & Sons, Ltd.: West Sussex, England, 2004.
5
6
7
8 56. Wiitala, K. W.; Hoye, T. R.; Cramer, C. J. *J. Chem. Theory Comput.* **2006**, *2*, 1085-1092.
9
10 57. Chung, T. F.; Wu, Y. M.; Cheng, C. H. *J. Org. Chem.* **1984**, *49*, 1215.
11
12
13
14
15
16
17
18
19
20
21
22
23
24
25
26
27
28
29
30
31
32
33
34
35
36
37
38
39
40
41
42
43
44
45
46
47
48
49
50
51
52
53
54
55
56
57
58
59
60